Received: 24 August 2023 | Revised: 15 February 2024 | Accepted: 21 February 2024

DOI: 10.1111/apha.14126

ACTA PHYSIOLOGICA

RESEARCH PAPER

Knock-out of dipeptidase CN2 in human proximal tubular cells disrupts dipeptide and amino acid homeostasis and para- and transcellular solute transport

Tilman Pfeffer[1,2] | Susanne M. Krug[3] | Tamara Kracke[1] | Robin Schürfeld[1] | Florian Colbatzky[1] | Philip Kirschner[1] | Rebekka Medert[4] | Marc Freichel[4] | Dagmar Schumacher[4] | Maria Bartosova[1] | Sotiris G. Zarogiannis[1] | Martina U. Muckenthaler[5,6,7,8] | Sandro Altamura[5,6] | Silvia Pezer[1] | Nadine Volk[9] | Constantin Schwab[10] | Stefan Duensing[11] | Thomas Fleming[12] | Elena Heidenreich[13] | Johannes Zschocke[14] | Rüdiger Hell[13] | Gernot Poschet[13] | Claus P. Schmitt[1] | Verena Peters[1]

[1]Medical Faculty Heidelberg, Center for Pediatric and Adolescent Medicine, Department I, Division of Pediatric Neurology and Metabolic Medicine, Heidelberg University, Heidelberg, Germany

[2]Tissue Bank of the German Center for Infection Research (DZIF), Partner Site Heidelberg, Institute of Pathology, Heidelberg University Hospital, Heidelberg, Germany

[3]Clinical Physiology/Nutritional Medicine, Charité-Universitätsmedizin Berlin, CBF, Berlin, Germany

[4]Institute of Pharmacology, Heidelberg University, Heidelberg, Germany

[5]Department of Pediatric Oncology, Hematology and Immunology and Hopp Children Cancer Center (KiTZ), University Hospital Heidelberg, Heidelberg, Germany

[6]Molecular Medicine Partnership Unit (MMPU), EMBL and University of Heidelberg, Heidelberg, Germany

[7]Translational Lung Research Center Heidelberg (TLRC), German Center for Lung Research (DZL), University of Heidelberg, Heidelberg, Germany

[8]DZHK (German Centre for Cardiovascular Research), Partner Site Heidelberg/Mannheim, Heidelberg, Germany

[9]Tissue Bank of the National Center for Tumor Diseases (NCT), Heidelberg, Germany

[10]Institute of Pathology, University Hospital Heidelberg, Heidelberg, Germany

[11]Department of Urology, University Hospital Heidelberg and National Center for Tumor Diseases (NCT) Heidelberg, Heidelberg, Germany

[12]Internal Medicine I and Clinical Chemistry, University Hospital Heidelberg, Heidelberg, Germany

[13]Centre for Organismal Studies (COS), University of Heidelberg, Heidelberg, Germany

[14]Institute of Human Genetics, Medical University of Innsbruck, Innsbruck, Austria

Correspondence
Verena Peters, Medical Faculty Heidelberg, Center for Pediatric and Adolescent Medicine, Department I, Division of Pediatric Neurology and Metabolic Medicine, Heidelberg

Abstract

Aim: Although of potential biomedical relevance, dipeptide metabolism has hardly been studied. We found the dipeptidase carnosinase-2 (CN2) to be abundant in human proximal tubules, which regulate water and solute homeostasis.

Tilman Pfeffer and Susanne M. Krug shared first authorship.

Claus P. Schmitt and Verena Peters shared senior authorship.

University, Heidelberg 69120, Germany.
Email: verena.peters@med.uni-heidelberg.de

Funding information
Elite Programme; Olympia Morata Program of Heidelberg University; Deutsche Forschungsgemeinschaft

We therefore hypothesized, that CN2 has a key metabolic role, impacting proximal tubular transport function.

Methods: A knockout of the CN2 gene (*CNDP2*-KO) was generated in human proximal tubule cells and characterized by metabolomics, RNA-seq analysis, paracellular permeability analysis and ion transport.

Results: *CNDP2*-KO in human proximal tubule cells resulted in the accumulation of cellular dipeptides, reduction of amino acids and imbalance of related metabolic pathways, and of energy supply. RNA-seq analyses indicated altered protein metabolism and ion transport. Detailed functional studies demonstrated lower *CNDP2*-KO cell viability and proliferation, and altered ion and macromolecule transport via trans- and paracellular pathways. Regulatory and transport protein abundance was disturbed, either as a consequence of the metabolic imbalance or the resulting functional disequilibrium.

Conclusion: CN2 function has a major impact on intracellular amino acid and dipeptide metabolism and is essential for key metabolic and regulatory functions of proximal tubular cells. These findings deserve in vivo analysis of the relevance of CN2 for nephron function and regulation of body homeostasis.

KEYWORDS
amino acids, dipeptidase, glutathione, ion transport, proliferation, proximal tubule

1 | INTRODUCTION

The role of dipeptide (DP) metabolism in health and disease has hardly been studied, and knowledge on its pathophysiological role is mainly limited to carnosine (β-Ala-His), even though significant biological functions have been demonstrated for other DPs such as Ala-Gln and Tyr-Asp.[1,2] One of the major dipeptidases in humans is carnosinase 2 (CN2, EC 3.4.13.18) encoded by the *CNDP2* gene.[3] CN2 has a negligible role in carnosine metabolism in vivo[4] but degrades cysteinyl-glycine in yeast and mice[5,6] and thyreonyl-serine in the human kidney.[7] CN2 forms N-lactoyl-amino-phenylalanine,[8] a signaling metabolite that suppresses feeding and obesity,[9] suggesting not only CN2 involvement in DP degradation but also extended regulatory functions within the body metabolism. *CNDP2* variants have been associated with the risk of diabetic nephropathy and disease progression in patients with type 2 diabetes[10,11] and changes in *CDNP2* expression have been associated with tumor disease.[12–14] *Cndp2*-KO mice exhibited aggravated progression of kidney damage after an acetaminophen overdose, probably related to increased ferroptosis.[6]

The human proximal tubule has a central role in water, ion and small nutrient transport,[15,16] is the primary location for renal gluconeogenesis[17] and plays a critical role in the progression of kidney disease.[18,19] Protein degradation and synthesis within the kidney are tightly regulated, and altered amino acid (AA) metabolism contributes to the progressive development of (chronic) kidney disease.[20–22] The cellular AA pool is determined by a tight balance between uptake, biosynthesis and protein catabolism, and AA are used for energy production and macromolecules such as proteins and glutathione.[23] In this context, the role of DP-degrading activity and its impact on AA availability in the kidney, however, has not yet been studied. We therefore investigated the relevance of CN2 for renal DP and AA metabolism. For this purpose, we generated a knockout of the CN2 gene (*CNDP2*-KO) in human proximal tubular cells, the main cell type of CN2 expression in the human kidney, and examined the impact on DP and AA concentrations and the effects on GSH metabolism, gluconeogenesis and energy production, protein biosynthesis and resulting impact on specific kidney cell function.

2 | RESULTS

2.1 | CN2 is abundant in human kidney proximal tubules

First, we analyzed CN2 expression within different organ tissues of mouse and human. CN2 was most abundant

in the kidneys of mouse and human, in particular in the proximal tubular segments, without differences between proximal tubular segments, and in smaller amounts also in distal tubules, parietal epithelial cells and glomerular cells (Figure 1). The most abundant DP in human kidneys were anserine, Asp-Gln, Gly-Asp, carnosine, and His-Ser, and the most abundant AA were glutamate, glycine, alanine and glutamine (Tables S1A,B). *CNDP2*-KO in HK-2 cells was established by CRISPR/Cas9 genome editing. After transfection, three independent *CNDP2*-KO clones (D10p1, H5p2 and H4p6) were identified with biallelic indel mutations leading to frameshifts and premature stop codons (Figure S1A). Western Blot analysis confirmed the absence of CN2 protein expression in all three clones compared to WT HK-2 cells and verified *CNDP2* deficiency in *CNDP2*-KO clones (Figure S1B). Subsequent experiments were performed with clone H4p6, in which metabolic degradation activity for the substrate Ser-Gln was almost abolished (Figure S1C). Specific markers for proximal tubular epithelium AQP1, SGLT2 and $NH3^+$ were present in WT and *CNDP2*-KO cells (Figure S2).

2.2 | Altered DP and AA metabolism in *CNDP2*-KO proximal tubular cells

To test then the extent to which CN2 plays a role in DP degradation in the cells, we compared the degradation rates of WT with those of *CNDP2*-KO (Table 1). Loss of CN2 function reduced degradation of 7 out of 21 DP studied and led to a marked (32%–86%) reduction of the concentration of all AA, which reached significance levels for >50% (11/19 AA). This effect was most marked for the highly abundant amino acids glutamate/glutamine (measured Glu may include des-aminated Gln), aspartate, serine, and alanine, but was also (highly) significant for cysteine and 5-oxoproline involved in the gamma-glutamyl cycle (Table 2). In contrast, there was a marked increase in the cellular concentration of most DP, with an

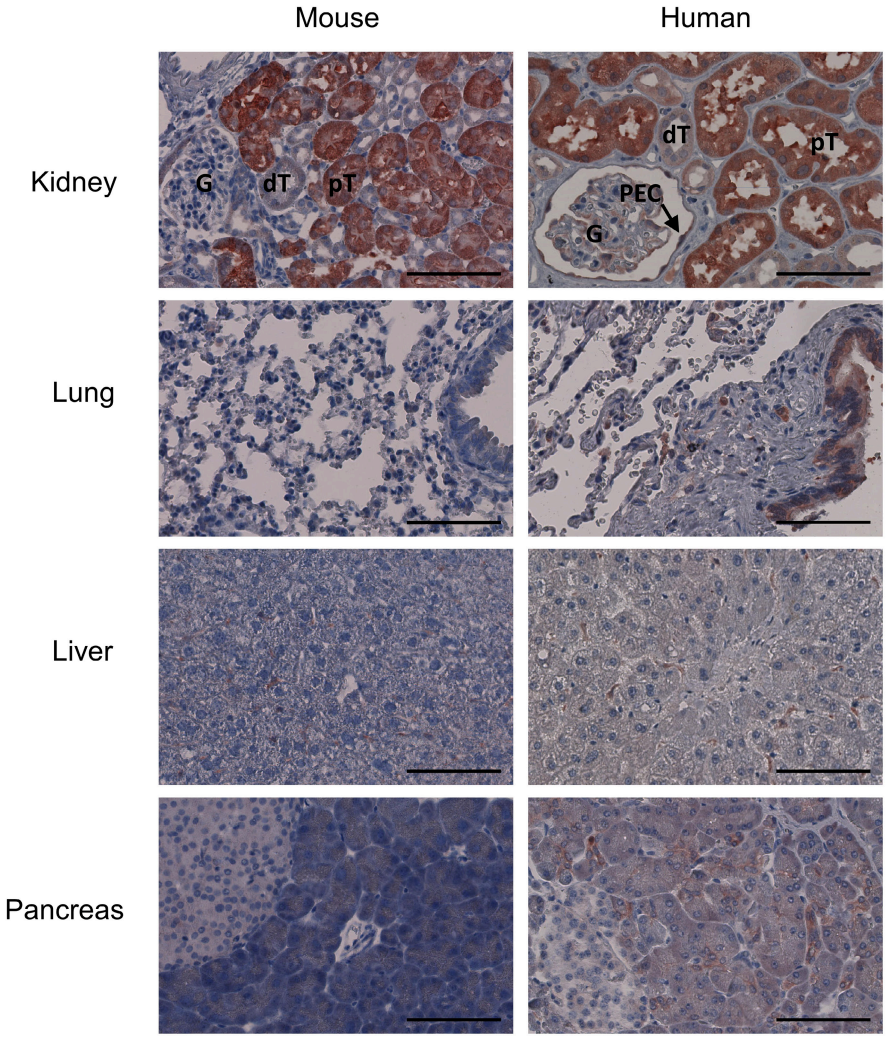

FIGURE 1 CN2 in human and mice kidney, lung, liver and pancreas. Immunohistochemical staining of CN2 (scale bar 100 μm) demonstrates high CN2 abundance in proximal tubules (PT) and lower abundance in distal tubules (dt), glomeruli (G) and parietal epithelial cells (PEC), while minor amounts can be detected in the other organs.

TABLE 1 DP concentrations and DP metabolic rates in WT and *CNDP2*-KO human proximal tubular cells.

	DP concentration					DP Metabolic rate		
	WT (pmol/mg)	*CNDP2*-KO (pmol/mg)	*p*	Log2 FC	FC	Activity WT (μmol/mg*h)	Activity *CNDP2*-KO (μmol/mg*h)	*p*
Cys-Gly	1.2 ± 0.5	3.1 ± 0.7	0.0001	1.42	2.68	1.26 ± 0.1	0.55 ± 0.03	0.001
Tyr-Phe	0.5 ± 0.3	1.0 ± 0.7	0.19	1.03	2.04	0.04 ± 0.03	0.08 ± 0.07	0.19
Gly-Glu	327.1 ± 297.6	656.2 ± 198.1	0.013	1.00	2.01	0.19 ± 0.1	0.14 ± 0.1	0.58
Ala-Glu	19.1 ± 8.9	37.5 ± 14.3	0.004	0.97	1.96	0.94 ± 0.3	0.09 ± 0.03	0.005
Val-Tyr	1.8 ± 0.5	2.4 ± 1.4	0.21	0.45	1.37	0.05 ± 0.04	0.04 ± 0.02	0.75
Gly-Asp	337.4 ± 111.0	439.4 ± 147.6	0.12	0.38	1.30	0.07 ± 0.01	0.02 ± 0.01	0.016
Anserine	337.9 ± 95.5	436.0 ± 138.3	0.10	0.37	1.29	0.04 ± 0.01	0.03 ± 0.02	0.89
Ser-Ala	6.8 ± 2.2	8.7 ± 3.0	0.15	0.35	1.28	1.68 ± 0.5	0.18 ± 0.1	0.003
Ala-Phe	1.5 ± 0.6	1.8 ± 0.7	0.23	0.32	1.25	0.15 ± 0.1	0.05 ± 0.02	0.21
Ala-Gln	10238.1 ± 5238.8	12704.9 ± 7703.6	0.44	0.31	1.24	12.57 ± 5.3	4.81 ± 0.9	0.07
Ala-Pro	8.4 ± 2.1	10.0 ± 4.8	0.37	0.25	1.19	0.25 ± 0.2	0.29 ± 0.2	0.82
Ala-Tyr	0.9 ± 0.4	1.1 ± 0.3	0.30	0.23	1.17	n.d.	n.d.	
Leu-Pro	5.8 ± 1.7	6.7 ± 1.9	0.35	0.19	1.14	0.41 ± 0.04	0.17 ± 0.05	0.003
Gly-Pro	19.1 ± 9.5	21.2 ± 5.6	0.58	0.15	1.11	0.9 ± 0.2	0.93 ± 0.5	0.94
Gly-Leu	18.3 ± 6.7	20.1 ± 2.4	0.63	0.14	1.10	n.d.	n.d.	
Pro-Gly	24.3 ± 5.9	26.4 ± 8.1	0.53	0.12	1.09	2.42 ± 0.6	1.08 ± 0.3	0.02
Tyr-Ala	0.7 ± 0.1	0.7 ± 0.5	0.83	0.10	1.07	n.d.	n.d.	
Ala-Ala	10.9 ± 2.8	11.5 ± 5.7	0.77	0.08	1.06	n.d.	n.d.	
Asp-Gln	52.0 ± 9.8	54.8 ± 21.6	0.73	0.08	1.05	0.22 ± 0.02	0.18 ± 0.02	0.57
Carnosine	78.9 ± 22.6	82.5 ± 36.7	0.81	0.06	1.04	0.03 ± 0.02	0.02 ± 0.01	0.82
His-Ser	62.7 ± 14.5	65.3 ± 26.4	0.80	0.06	1.04	0.03 ± 0.05	0.05 ± 0.03	0.63
Glu-Glu	52.3 ± 15.2	53.3 ± 25.7	0.92	0.03	1.02	n.d.	n.d.	
His-Ala	19.4 ± 24.8	19.7 ± 29.5	0.98	0.02	1.02	n.d.	n.d.	
Pro-Leu	1.2 ± 0.5	1.1 ± 0.4	0.85	−0.07	0.95	1.48 ± 0.8	2.44 ± 2.2	0.51
Ser-Gln	6.3 ± 2.0	5.9 ± 2.2	0.69	−0.10	0.94	1.95 ± 0.3	0.07 ± 0.02	0.001
Ala-Gly	7.1 ± 3.4	6.4 ± 4.0	0.68	−0.16	0.89	0.06 ± 0.01	0.07 ± 0.03	0.68
Gly-Phe	3.2 ± 0.6	2.9 ± 1.6	0.54	−0.16	0.89	n.d.	n.d.	
Gly-His	10.4 ± 5.2	9.0 ± 3.2	0.52	−0.20	0.87	n.d.	n.d.	
Phe-Ala	0.7 ± 0.3	0.6 ± 0.3	0.52	−0.27	0.83	n.d.	n.d.	
Leu-His	1.7 ± 1.7	1.0 ± 0.00	0.35	−0.85	0.56	0.61 ± 0.1	0.61 ± 0.1	0.94
His-Leu	0.7 ± 0.6	0.2 ± 0.00	0.15	−1.58	0.33	n.d.	n.d.	

Note: Dipeptide (DP) profile and degradation rates in WT and *CNDP2*-KO human proximal tubular epithelial cells (HK-2). Metabolic rates were reduced for 7 of 21 DP ($p < 0.05$). FC, fold change, data are mean and SD, $n = 4–9$.

TABLE 2 AA concentrations in WT and *CNDP2*-KO human proximal tubular epithelial cells.

	AA in WT (µmol/mg)	AA in *CNDP2*-KO (µmol/mg)	*p*-value	Log2 (FC)	FC	% reduction in KO
Gln	8.9 ± 4.2	1.3 ± 0.2	0.022	−2.83	0.14	86
Asp	28.0 ± 5.7	4.1 ± 0.8	0.0001	−2.77	0.15	85
Ser	35.6 ± 6.0	10.5 ± 2.9	0.001	−1.77	0.29	71
Glu	823.0 ± 163.6	309.8 ± 74.1	0.002	−1.41	0.38	62
Ala	54.1 ± 12.6	22.1 ± 5.5	0.007	−1.29	0.41	59
Cys	11.1 ± 4.5	5.5 ± 1.1	0.004	−1.02	0.49	51
Val	4.6 ± 0.7	2.4 ± 0.3	0.001	−0.97	0.51	49
His	36.1 ± 7.9	19.5 ± 4.8	0.017	−0.89	0.54	46
Tyr	2.0 ± 0.5	1.2 ± 0.3	0.054	−0.76	0.59	41
Leu	6.1 ± 1.5	3.7 ± 0.9	0.048	−0.74	0.60	40
Arg	11.4 ± 3.7	6.8 ± 1.6	0.093	−0.74	0.60	40
Phe	1.9 ± 0.4	1.2 ± 0.5	0.068	−0.68	0.62	38
Ile	5.2 ± 1.4	3.2 ± 0.9	0.073	−0.70	0.62	38
Thr	16.9 ± 2.5	11.0 ± 3.1	0.023	−0.62	0.65	35
Gly	23.2 ± 3.7	15.9 ± 3.4	0.031	−0.55	0.68	32
Asn	25.1 ± 5.4	17.2 ± 5.1	0.087	−0.55	0.69	31
Met	2.2 ± 0.5	1.5 ± 0.5	0.138	−0.49	0.71	29
Lys	3.1 ± 0.8	2.4 ± 0.7	0.231	−0.39	0.76	24
Pro	30.3 ± 4.9	26.8 ± 8.8	0.484	−0.18	0.88	12

Note: Amino acid (AA) profile of WT and *CNDP2*-KO human proximal tubular cells (HK-2). 11 of 19 amino acids were reduced in *CNDP2*-KO cells. FC, fold change, data are mean and SD, $n = 3–5$.

increase by 25%–101% for the highly abundant dipeptides (concentration >100 pmol/mg: Gly-Glu, Gly-Asp, anserine and Ala-Gln) and reached 168% for cysteinylglycine (Cys-Gly) which plays a major role in the gamma-glutamyl cycle. Cys-Gly, Gly-Glu and Ala-Glu were significant, twofold increased. The CN2-dependent DP accumulation is in line with the central role of CN2 in cellular DP metabolism. *CNDP2*-KO caused a marked reduction in the DP metabolic rate, which was most significant for Cys-Gly cleavage (Table 1). Although the DP degradation was reduced for several DPs in the *CNDP2*-KO, the degradation rate was not fully abolished, indicating the activity of further dipeptidases. Recombinant CN2 also has a broad DP substrate range and high DP degradation rates (Table S2); degradation efficiency (V_{max}/K_M) was high for Cys-Gly and Ser-Gln, and 540- and 160-fold lower for carnosine (Table S3). The human kidney degradation rate for Ser-Gln was 19.4 ± 8.8 nmol/mg·h and for carnosine only 3.5 ± 2.4 nmol/mg·h, despite the presence of CN1 in the human kidney tissue. We then studied putative regulatory mechanisms of CN2 activity. Cys-Gly dose-dependently decreased Ser-Gln degradation by rCN2 and vice versa Ser-Gln reduced Cys-Gly degradation rate, suggesting an interacting inhibitory feedback loop on CN2 activity; GSH had a DP substrate-specific effect (Figure S3).

2.3 | Secondary metabolic alterations in *CNDP2*-KO proximal tubular cells

In line with a reduced concentration of the important gamma-glutamyl cycle amino acids (Cys, Gly, 5-oxoproline, Glu) and increased Cys-Gly, *CNDP2*-KO also led to a significant reduction of glutathione concentrations both in the reduced (GSH) and oxidized (GSSG) state (by 60% and 80%, Figure 2). In the presence of redox stress, loss of CN2 function was not associated with a reduced GSH/GSSG ratio (87:1 in WT and 200:1 in *CNDP2*-KO cells). In line with this, the NAD/NADPH ratio—a measure of redox status—and malondialdehyde, a marker of lipid peroxidation, were not different in *CNDP2*-KO and WT cells (Table S4). Exogenous oxidative stress did not further reduce *CNDP2*-KO cell viability than in WT cells (Figure S4A). Cys-Gly, which accumulated in the *CNDP2*-KO cells and has a high antioxidative capacity (Figure S4B), may have compensated for the alterations in the glutathione pathway. *CNDP2*-KO-cells, however, were more sensitive to Cisplatin, which interferes with DNA replication, and cell viability was consistently reduced compared to WT cells (Figure S4C).

20% of human gluconeogenesis occurs in the kidney. Among the reduced AA in *CNDP2*-KO cells, nine are

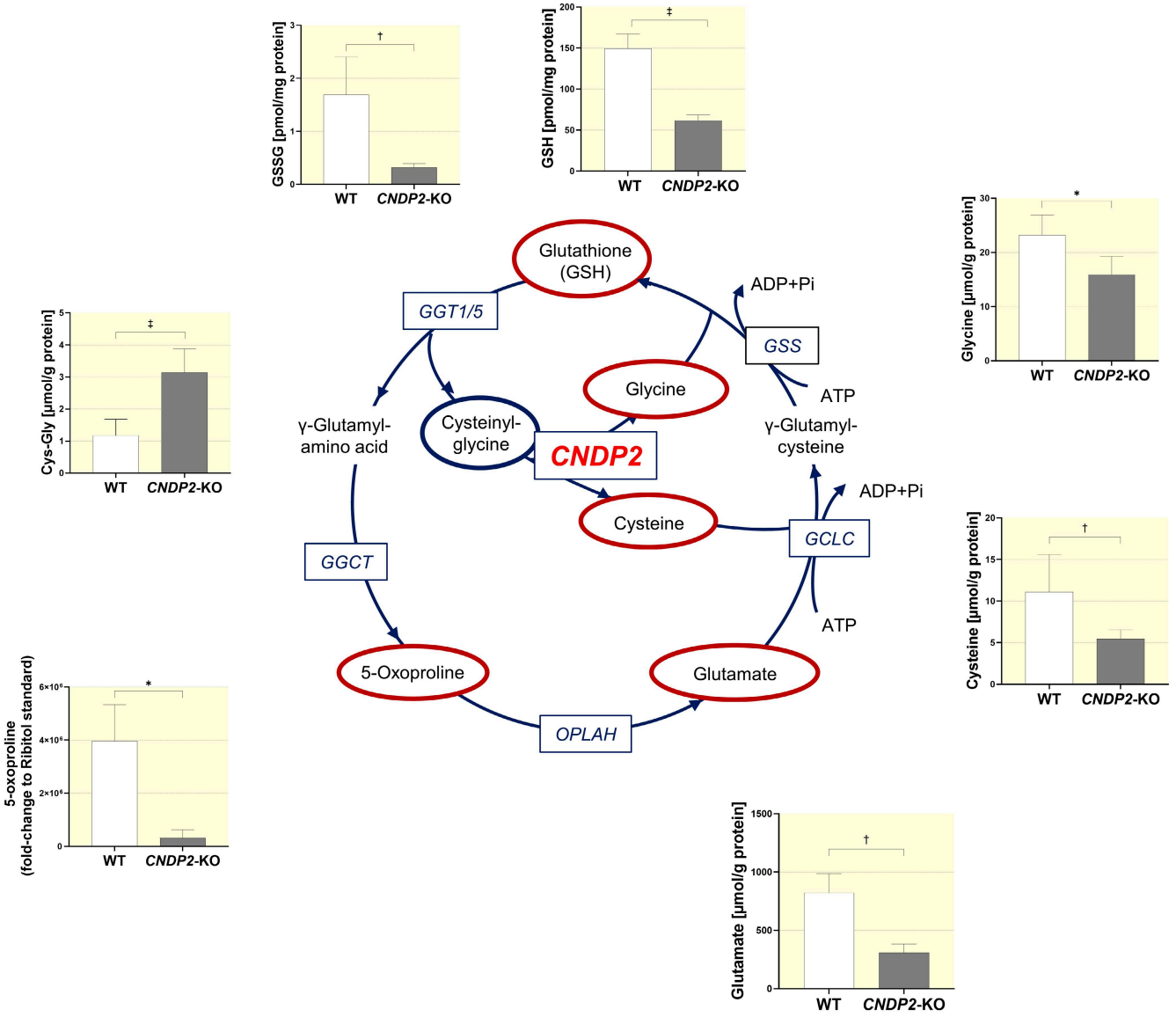

FIGURE 2 CN2 dependent alterations in the glutathione pathway of human proximal tubular cells. *CNDP2*-KO in HK-2 cells reduced GSSG (−80%), GSH (−60%), Glycine (−32%), cysteine (−50%), glutamate (−62%), and 5-oxoproline (−92%), whereas Cys-Gly concentrations were 3-fold increased compared to WT cells. Data are mean and SD, $n = 3–8$. *$p < 0.05$, †$p < 0.01$; ‡$p < 0.001$ (unpaired *t*-test).

glucogenic (Gln, Asp, Ser, Glu, Ala, Cys, Val, His, and Gly), together with a reduced pyruvate concentration in compared to WT cells, while glucose and glycerol-3P concentrations were not altered. Energy status was reduced, that is, AMP/ATP and ADP/ATP ratios were increased (Table S4). The concentration of myo-inositol, a carboxylic sugar derivate, was reduced in *CNDP2*-KO compared to WT cells. In downstream metabolic pathways, expression of myo-inositol oxygenase (*MIOX*) mRNA was doubled, while Inositol-3-phosphate (*MIPS*) and Inositol monophosphatase (*IMPA 1*) were not altered (Figure S5). Lipidomic analysis of *CNDP2*-KO cells demonstrated differences in the glycerophospholipid composition, total glycerophospholipid concentration was unchanged ($p = 0.6$). Glucosylceramides were decreased (Figure S6, Table S5).

2.4 | *CN2*-dependent alterations of proximal tubular cell viability

CNDP2-deficient cells were phenotypically altered, that is, were larger (forward scatter: 233 ± 3 vs. 197 ± 2), and displayed higher granularity (side scatter 190 ± 1.1 vs. 215 ± 5.7; two-way ANOVA both $p < 0.0001$; Figure 3A). *CNDP2*-KO cell viability was 25% and 50% lower than that of WT cells after 24 and 48 h, proliferation rate was reduced, readily explaining the time-dependent differences

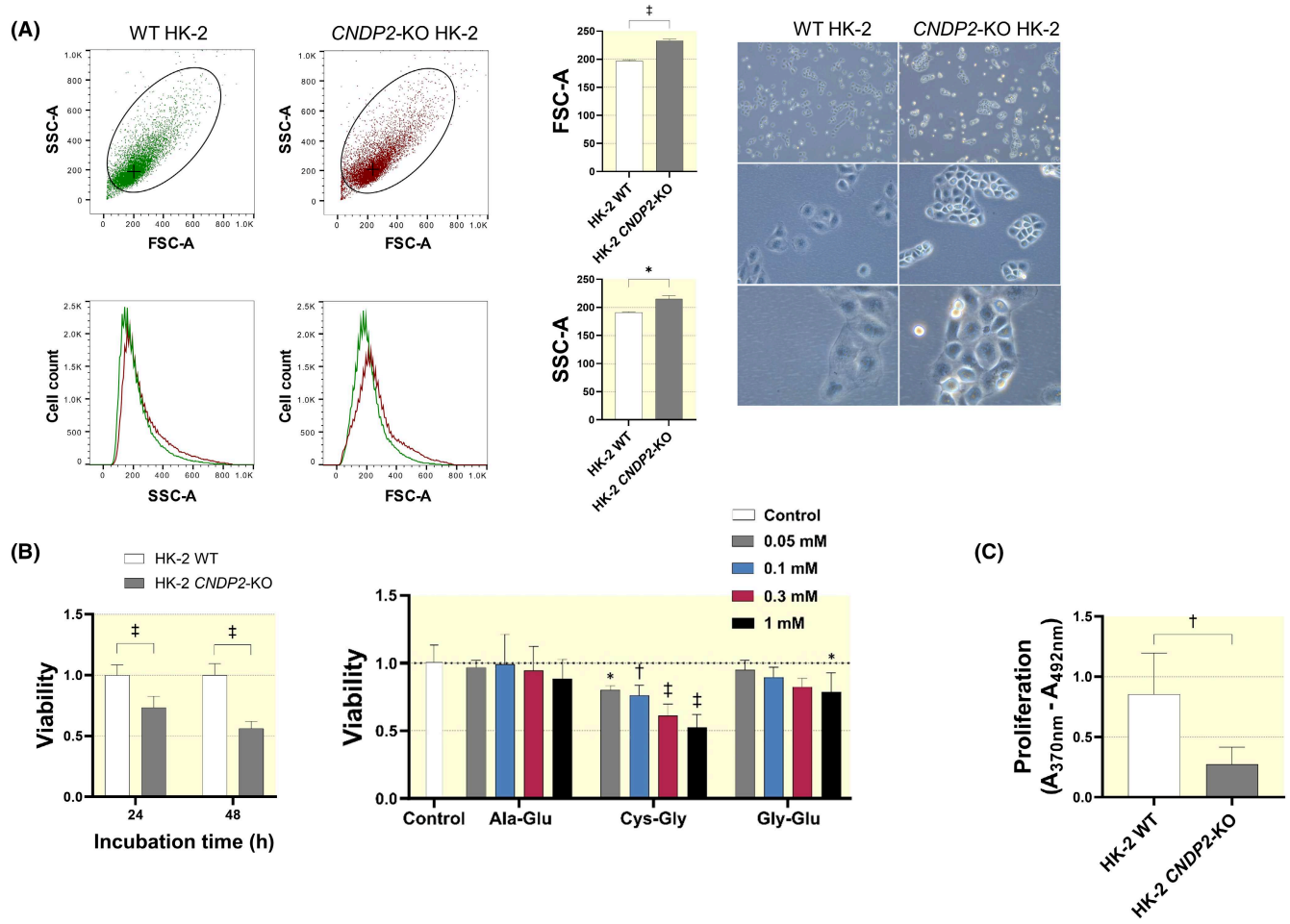

FIGURE 3 *CNDP2*-KO and WT human proximal tubular cells morphology, viability and proliferation rate. (A) Forward and side scatter (FSC/SSC) profiles demonstrate increased size and granularity of *CNDP2*-KO HK-2 cells compared to WT cells (FACS, $n = 3$); representative phase contrast light microscopy images are given on the right (5-, 20-, 40-fold magnification). (B) Cell viability was decreased in *CNDP2*-KO (white bar) compared to WT cells (black bars, 0.1% FCS, MTT assay; $n = 16$), and in WT cells dose dependently reduced with two of the three DP most accumulated in *CNDP2*-KO cells, $n = 3$. (C) Proliferation rates were reduced by the *CNDP2*-KO (BrdU-assay), $n = 5$. Data are mean and SD, $*p < 0.05$, $\dagger p < 0.01$, $\ddagger p < 0.001$ (unpaired *t*-test).

in viable cell counts between WT and KO cells. In WT cells, the DP Cys-Gly and Gly-Glu, accumulating in *CNDP2*-KO cells dose-dependently reduced viable cell counts, demonstrating detrimental effects of the DP accumulation (Figure 3B,C).

In contrast, supplementation of the 11 most depleted AA and myo-inositol for 48 h did not restore viable *CNDP2*-KO cell counts (Table S6), indicating non-reversibility of the metabolic depletion-induced effects. Likewise, the activity of caspase-3 was 1.0 ± 0.1 relative to control in both WT and KO cells, excluding an impact of caspase-dependent cell apoptosis. We did not find evidence of ferroptosis in *CNDP2*-KO proximal tubular cells. Expression of ferroptosis-related prostaglandin-endoperoxide synthase 2 (*PTGS2*) was reduced to <1% ($p < 0.0001$) and the ferroptosis inhibitor ferrostatin (0.1–0.3 μM) did not improve *CNDP2*-KO cell viability. Iron stress (ammonium ferric citrate, 0.05–0.4 mM) did not further reduce cell viability of KO cells than in WT cells.

2.5 | Altered biological processes in *CNDP2*-KO human proximal tubular cells

We analyzed how the KO of CN2 affected biological processes by RNA-seq. GO term analysis of differentially regulated genes demonstrated upregulation of the biological processes' ion transport, positive regulation of cell communication, cell adhesion and cell junction organization, while regulation of localization, cell development, locomotion and regulation of ion transport were downregulated (Figure 4). KEGG pathway analysis indicated alterations in pathways related to "protein digestion and absorption" (hsa04974) and "amino

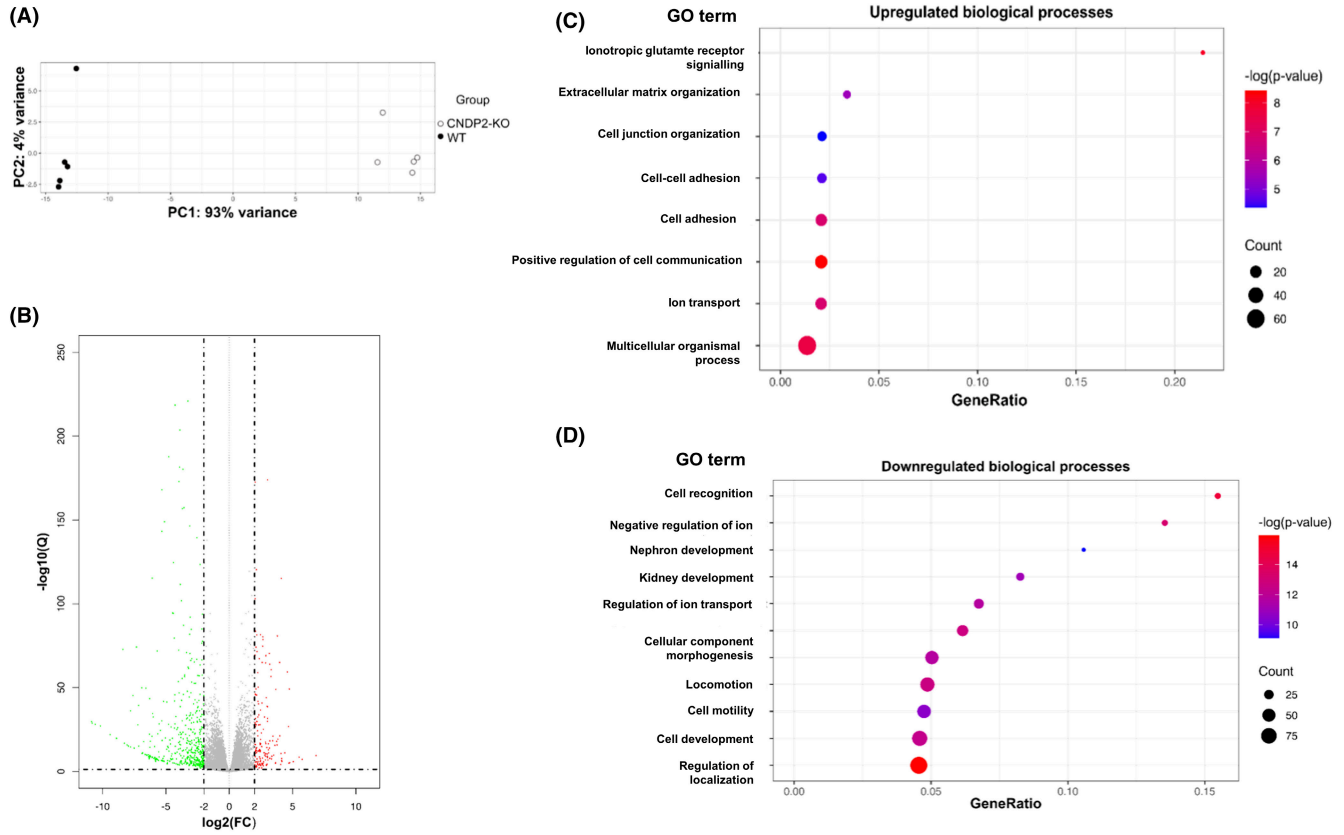

FIGURE 4 Gene and biological pathway regulation in *CNDP2*-KO human proximal epithelial cells. (A) Principal component analysis revealed difference between *CNDP2*-KO and WT HK-2 cells with a clustering of the individual replicates. (B) Up- and down-regulated genes in *CNDP2*-KO HK-2 vs. WT cells ($n = 5$). The vertical dashed lines indicate 4-fold increased, the horizontal dashed line displays –log10(0,1) = 1. (C) Upregulated and (D) downregulated biological processes are displayed regarding their GeneRatio, significances as –log(*p*-value) and the number of significant altered genes.

acids" (hsa00330, hsa00380). We therefore also analyzed other dipeptidases and DP transporters. Expression of dipeptidyl peptidase 3 (*DPP3*) and peptidase D (*PEPD*) were reduced by 40% (both $p < 0.0001$) in *CNDP2*-KO cells, but not of dipeptidase 1 (*DPEP1*) and *DPP 4, 7, 8, 9*. Expression of the dipeptide transporter PHT2 (*SLC15A3*) was 1.6-fold upregulated in KO cells, PEPT2 (*SLC15A2*), PHT1 (*SLC15A4*) and Cubilin (*CUBN*) were similar in *CNDP2*-KO and WT cells. DPEP2 and 3 and PEPT1 (*SLC15A1*) were not expressed in HK-2 cells.

2.6 | CN2-dependent trans- and paracellular ion and solute transport

To understand the consequence of *CNDP2*-KO-induced metabolic changes, we studied key transport functions of proximal tubular cells. General ion permeability, assessed by transepithelial resistance (TER) measurement, was higher in *CNDP2*-KO HK-2 cells over time and reached a two-fold higher plateau level than WT cells after 9 days (39.9 ± 6.9 vs. $22.5 \pm 2.9\,\Omega \cdot cm^2$ in WT cells, $p < 0.0001$, Figure 5A). Incubation of WT cells with the three DP accumulating most in the *CNDP2*-KO cells (Ala-Glu, Cys-Gly and Gly-Glu) at 0.33- and 1-mM concentrations increased TER (Figure 5B), suggesting that this accumulation due to disturbed DP degradation in the *CNDP2*-KO increased TER.

As TER reflects ion permeability, we measured trans- and paracellular main ion permeabilities across key transcellular ion transporters. Cystic Fibrosis Transmembrane Conductance Regulator (CFTR; chloride-transport) and SGLT1/2 (sodium-glucose transporter 1 and 2) function were unaffected by the *CNDP2*-KO (Figure 6A). In contrast, the activity of the sodium-proton-exchangers (NHE) was increased (Figure 6B), suggesting also alterations of the acid–base regulations and activity of proton-driven DP transport via peptide transporters like PepT2. Dilution potential measurements demonstrated higher cation selectivity in *CNDP2*-KO HK-2 cells than in WT cells, as the ratio P_{Na}/P_{Cl} increased (1.17 ± 0.09 vs. 2.00 ± 0.20, $n = 11;16$, $p < 0.01$, Figure 6C). This change was based on a reduced permeability for chloride, while the permeability for sodium was unaffected (Figure 6D). Analyzing permeability

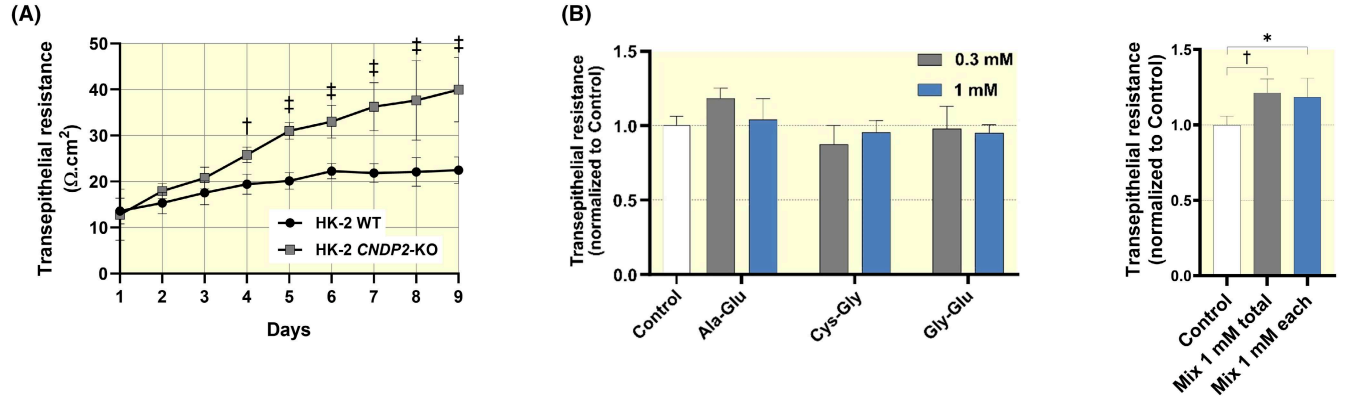

FIGURE 5 Transepithelial resistance and paracellular macromolecule transport in *CNDP2*-KO and WT human proximal tubular cells. (A) Transepithelial resistance, a measure of ion permeability, was increased in *CNDP2*-KO HK-2 cells compared to WT cells ($n = 10$–11) and (B) increased in WT cells when exposed to the combination of the three DP most accumulated in the KO cells. Data are mean and SD. *$p < 0.05$, †$p < 0.01$, ‡$p < 0.001$ (unpaired *t*-test).

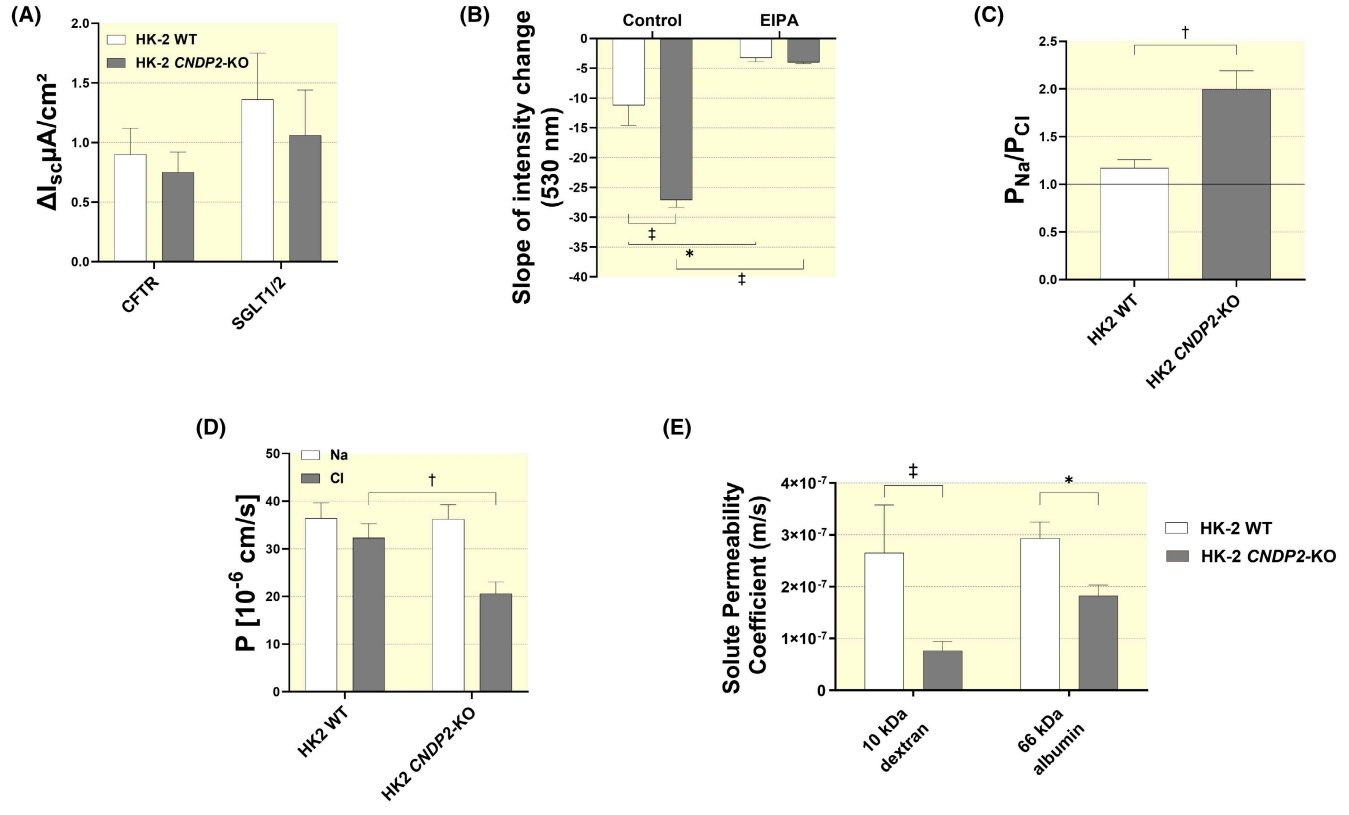

FIGURE 6 Ion transport in *CNDP2*-KO and wild type human proximal tubular cells. (A) CFTR activity (transport of Cl^-) and glucose transport via SGLT1/2 were unaltered in *CNDP2*-KO HK-2 cells ($n = 6$–9), whereas (B) the activity of the sodium-proton-exchangers (NHE) was increased, but blocked by NHE inhibitor EIPA ($n = 10$; 12). (C) Ion selectivity in *CNDP2*-KO was increased towards cations ($n = 11$; 16) and (D) the permeability for chloride was almost halved. (E) Macromolecule transport was lower in *CNDP2*-KO cells ($n = 3$; 6). Data are mean and SD. *$p < 0.05$, †$p < 0.01$, ‡$p < 0.001$ (unpaired Student's *t*-test, in (B) with correction for multiple testing (Bonferroni-Holm).

for macromolecules in *CNDP2*-KO cells, we found reduced permeability coefficients for the paracellular flux markers 10 kDa dextran and 66 kDa albumin (71.1 ± 6.0% and 37.9 ± 6.6%; $p < 0.05$, <0.0001) in comparison to WT cells (Figure 6E).

Paracellular transport of ions, solutes and water is determined by the composition of tight junction (TJ) proteins. We therefore analyzed TJ expression in the proximal tubular cells. CLDN2, CLDN8, and ILDR2 were reduced, while CLDN1 and CLDN3 protein expression were increased

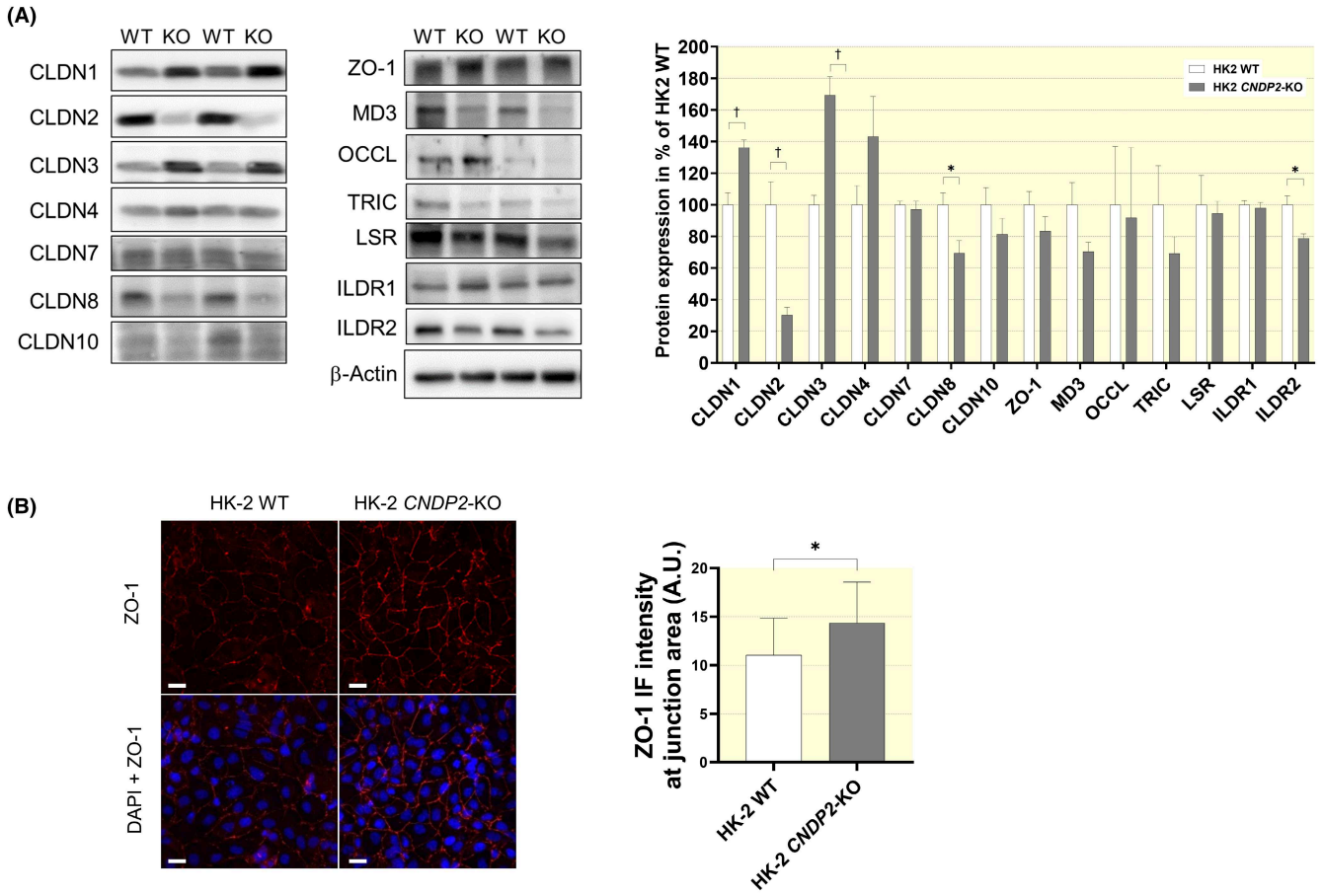

FIGURE 7 Tight junction protein expression and location in *CNDP2*-KO and wild type human proximal tubular cells. (A) Expression of tight junction proteins Claudin 2 and 8 (CLDN2 and 8) and of Immunoglobulin Like Domain Containing Receptor 2 (ILDR2) was decreased and of CLDN 1 and 3 was increased in *CNDP2*-KO cells compared to WT. Representative western blots and quantifications of 4 blots are given. Full blots are deposited in supplementary file. (B) Immunofluorescence staining of scaffolding protein zonula occludens-1 (ZO-1) demonstrates increased membrane ZO-1 abundance in *CNDP2*-KO cells ($n = 4$). Data are mean and SEM. $^*p < 0.05$, $^\dagger p < 0.01$ (unpaired Student's *t*-test).

in *CNDP2*-KO versus WT HK-2 cells (Figure 7A). ZO-1, a scaffolding protein of the TJ, was not changed in abundance, but increasingly localized in the membrane of the *CNDP2*-KO cells suggesting a higher TJ network integrity (Figure 7B).

3 | DISCUSSION

Knowledge on the DP metabolism in health and disease is mainly limited to carnosine and CN1, even though significant biological functions have been demonstrated for other DPs such as Ala-Gln and Tyr-Asp.[1,2] We now demonstrate that CN2 degrades carnosine only to a minor extent, in line with previous findings.[24] In contrast, both recombinant and proximal tubular cell CN2 have a broad specificity for degradation of a variety of DP, with high degradation rates. Depending on the DP, degradation rate was 4- to 300-fold higher than the degradation of carnosine by recombinant human CN1,[25] by CN1 in human proximal tubular epithelial cells and by human kidney tissue.[26] This underlines the metabolic importance of CN2 for the kidney and its potential as a key candidate regulating DP-dependent cellular functions.

CN2 is ubiquitously expressed with high levels found within the kidney.[6] We show that within the human kidney, CN2 is present in parietal glomerular epithelial cells that are essentially involved in glomerular regeneration and scarring,[27] and to be highly abundant in human proximal tubules, that reabsorb the vast majority of freely filtered solutes.[15] We did not observe differences in CN2 abundance across the proximal tubular segments. Recent kidney single-cell studies confirm *CNDP2* expression in the proximal tubules in different clusters (human protein atlas), but mRNA levels do not necessarily reflect protein abundance. Besides most ions and water, nutrients are completely reabsorbed here; carbohydrates like glucose,

but also AA and DP, and the highly abundant CN2 may play a critical metabolic role within the proximal tubular cells. In line with this notion, *CNDP2*-KO in human proximal tubular cells increased cellular concentrations of the majority of DP, but without a complete breakdown of DP degradation, which suggests partial compensation by other dipeptidases. We identified seven further dipeptidases beyond CN1 and CN2, of which DPP3 and PEPD were downregulated in *CNDP2*-KO, which may explain the observed discrepancies in the accumulation of several DP and their CN2-dependent metabolic rate.

Together with the altered cellular DP profile, the AA profile was markedly affected in *CNDP2*-KO cells, with 11 of 19 measured AA being reduced. This indicates a strong impact of CN2 on cellular AA availability, by high rate degradation of the different DP, present at about 1000-fold lower cellular concentrations than AA. These findings are also in line with previously reported correlations of the organ-specific DP profiles in mice with their respective AA concentrations.[28] The cellular AA pool is determined by a tight balance between uptake, biosynthesis and protein catabolism and plays a central role in energy production, macromolecule formation, and for glutathione synthesis and thus in the regulation of fundamental cellular processes.[29,30] Cellular uptake of dipeptides occurs by proton-coupled oligopeptide transporters (POTs) via an inwardly-directed proton gradient and negative membrane potential. At present, four members of the POT family, namely PEPT1 (SLC15A1), PEPT2 (SLC15A2), PHT1 (SLC15A4) and PHT2 (SLC15A3), have been identified in mammals.[31,32] PEPT1 and PEPT2 are expressed at the apical surface of epithelial cells from the kidney.[33–35] In the proximal tubule, megalin and the cubilin/amnionless receptor mediate the uptake of filtered proteins that escape the glomerular filtration barrier;[36] however, the role of megalin and cubilin in renal dipeptide transport needs further investigations. According to our RNA-seq data, *SLC15A2* (PEPT2), *SLC15A3* (*PHT2*)) and *SLC15A4* (PHT1) and cubilin (*CUBN*) are expressed in the proximal tubular cells, with a higher expression of *SLC15A3* in KO compared to WT cells.

Additional metabolic alterations secondary to *CNDP2*-KO relate to glucose and energy metabolism. 20% of human gluconeogenesis occur in the kidney, the proximal tubule is the primary location for renal gluconeogenesis.[37] Nine glucogenic AA were reduced, as was the pyruvate concentration and the energy status in *CNDP2*-KO compared to WT cells. Cellular glucose and glycerol-3P concentrations were not altered, which, however, may be due to a lack of gluconeogenic activity in the HK2 cells and greater effects might occur in vivo. Proximal tubular cells are highly energy-dependent.[19] These findings, together with the alterations in downstream metabolites and in the lipid profiles deserve further studies. The AA cysteine, glycine and glutamate, composing glutathione and 5-oxoproline, another component of the glutathione cycle, were reduced, readily explaining the lower cellular concentrations of GSSG and GSH. In vitro studies support the finding that CN2 is involved in cysteine recycling and the redox homeostasis of tubular cells.[6] The reduced glutathione levels of *CNDP2*-KO cells, however, did not result in a higher sensitivity to oxidative stress, possibly due to the intracellular accumulation of Cys-Gly, which we demonstrate to have high antioxidative action, similar to N-acetylcysteine. However, cell viability reduction by cisplatin, a chemotherapeutic agent interfering with DNA replication, was more pronounced in *CNDP2*-KO than in WT cells, a finding of potential relevance in cancer treatment. The therapeutic use of GSH in tumor diseases under cisplatin treatment is debated, as the conjunction of GSH with cisplatin may reduce the efficacy of Cisplatin.[38] The previously suggested link of the *CNDP2*-KO and altered glutathione status to ferroptosis[6] could not be reconfirmed in the human proximal tubular *CNDP2*-KO cells. Of note, the immortalized HK-2 cells, albeit widely used, may only partially reflect metabolic functions, different results may be obtained with primary human proximal tubular epithelial cells in vitro, and in kidneys in vivo.

Knock-out of *CNDP2* resulted not only in major metabolic alterations but also deteriorated essential proximal tubular cell functions, including para- and transcellular solute transport. RNA-seq analyses revealed several biological functions being affected by the *CNDP2*-KO, including cell adhesion, communication, junction organization and ion transport. In addition, the viability and proliferation rate of the *CNDP2*-KO cells were reduced, which we were able to link to the accumulation of DP. In WT cells, Cys-Gly, accumulating in *CNDP2*-KO cells, dose-dependently reduced cell viability, and supplementation of depleted AAs, or myo-inositol did not restore the viability of the *CNDP2*-KO cells, pointing to a more complex metabolic imbalance and irreversible alterations, respectively. Consistent with the notion of Cys-Gly induced cytotoxicity, in hepatoma-derived cells, CN2 knock-down reduced Cys-Gly turnover and cell viability.[6]

The metabolic shifts in DP and AA concentrations in CN2 deficient proximal tubular cells also affected the transport for ion and macromolecular solutes as suggested by the KEGG analysis. General ion permeability is reflected by the TER, which we found to be increased in the *CNDP2*-KO, also indicating a tightening effect with enhanced barrier properties. Again, a DP-dependent effect is suggested by the increased TER of WT cells incubated with three DPs accumulating in the *CNDP2*-KO

cells. Permeability for macromolecules (10 and 66 kDa) was reduced. Within the nephron under physiological conditions, 10 kDa molecules pass the intact glomerular filter and undergo tubular reabsorption. The much bigger albumin (66 kDa) only passes the filter in disease settings representing an early sign and pathomechanisms of nephropathy in the majority of patients.[39] The decreased permeability for macromolecules suggests a tightening of the epithelium, lowering uptake in response to the DP accumulation.

As the proximal tubule is a leaky epithelium, high transport rates not only occur via the large number of transporters facilitating transcellular uptake, but take place to even higher extent via the paracellular pathway, which is determined by tight junction proteins, mainly by the composition of members of the claudin family.[40] We found CLDN2 and CLDN8 to be markedly reduced and CLDN1 and 3 to be increased, which could lead to the observed changes in ion permeability. While CLDN1 and CLDN3 are barrier-enhancing claudins without any charge selectivity,[41,42] CLDN2 is forming paracellular channels for cations and water.[43] Its downregulation should enhance the barrier against cations but we observed rather cation-selective permeability in the *CNDP2*-KO cells. As CLDN8 is forming selective paracellular barriers against cations,[44,45] its downregulation could counterbalance the effects that were expected due to CLDN2 downregulation, leading to an apparent permeability reduction only for anions, although both were affected on paracellular level. Other tight junction proteins of relevance for ion permeability within the proximal tubule were not affected.

However, though not changed in expression, we observed an increased abundance of the scaffolding protein ZO-1 at the membrane of the *CNDP2*-KO cells, suggesting higher tight junction network integrity and stability, which again supports the finding of an enhanced barrier. Furthermore, ZO-1 is an important factor for osmotic pressure regulation of cell volume[46] and has tension-dependent functions for epithelial stability.[47] Changes in ZO-1 enrichment together with the observed changes in ion, DP and AA concentrations might also affect intracellular osmotic pressure. This assumption is supported by the observed upregulation of MIOX, an enzyme which is exclusively expressed in the kidney proximal tubule[48] and up-regulated by hyperosmotic stress.[49] Altered osmotic pressure may in turn further affect ion and solute transport. On the transcellular level, we did not find changes in CFTR and SGLT 1/2 transport activities but observed higher activity of the NHEs. In the proximal tubule, NHE1, NHE3, NHE4 and NHE8 are expressed within the apical or basolateral cell membrane and function as cation-proton antiporters.[50] They are involved in cell volume and cellular pH regulation, again pointing to altered osmotic pressure. In addition, the proton transport by NHEs links these transporters to di- and tripeptide uptake via for example PepT2, possibly contributing to the alterations in DP and AA profiles observed with the lack of CN2. The increased NHE activity may represent a regulatory response to the altered peptide metabolism and the assumed hyperosmotic pressure.

3.1 | Implications for pathological significance and outlook

Despite the limitations of in vitro cell models studied in limited number of independent experiments, the consistent and major alterations of DP and AA abundances and of associated metabolic pathways in CN2 deficient tubular cells together with markedly comprised cell functions including ion and large solute transports, suggest far reaching impact of CN2, which deserve subsequent in vivo studies. In complex In vivo systems, the CN2 activity may have a very different impact than in vitro in the human proximal tubular epithelial cells. In context of the nephron, dysregulation of CN2 might affect the whole body, as the kidney has important regulatory functions not only in reabsorption of ions and nutrients or excretion of metabolic end products and toxins, but also in regulation of acid–base-homeostasis and of blood pressure. Ion transport along the nephron regulates extracellular volume and blood pressure.[51] The proximal tubule plays a critical role in the progression of kidney disease,[18] CN2-related dysfunction may impact outcomes in patients with hypertension, diabetes and chronic kidney disease, where genetic variants of *CNDP2* already have been linked to outcome.[10,11] Also, the role of CN2 present in human parietal glomerular epithelial cells, which play a key role in glomerular regeneration,[27] deserves in-depth analyses. Additionally, the association of CN2 expression to tumors[12–14] might be well-connected to altered regulations in metabolism, which we here observed on cell culture level, but which in organs might influence tumor development and progression.

4 | MATERIALS AND METHODS

Chemicals were purchased from Sigma-Aldrich (Schnelldorf, Germany) unless indicated otherwise.

4.1 | Cell culture

Immortalized human tubular cells (HK-2; American Type Culture Collection CRL-2190) were grown in RPMI

1640 GlutaMAX medium (Thermo Fisher Scientific, Waltham, MA) with 0.1 or 10% fetal calf serum (v/v) and 1% penicillin and streptomycin (v/v) at 37°C with 5% CO_2. Experimental settings were performed in 0.1% fetal calf serum media, whereas 10% fetal calf serum media was used to adhere the cells after splitting. Cells were splitted using 0.25% trypsin (Thermo Fisher Scientific, Waltham, MA) and were used from passage 1 to 16.

4.2 | sgRNA selection and cloning

A gRNA targeting exon4 (specific recognition site, 5′-CGTGTGCATTTACGGG CACCT-3′) of the human *CNDP2* locus was designed using CRISPOR (http://crispor.tefor.net/) (PMID: 27380939) and cloned into a U6 promoter driven expression vector px549 pSpCas9(BB)-2A-Puro (Addgene plasmid #48139) according to the protocol described.[52] sgRNA transfection was performed with a resistance gene against puromycin and transfected cells were selected with puromycin (3 μg/mL) for 5 days. As confirmation for successful clone generation, absence of CN2 protein was analyzed by Western blotting.

4.3 | Sequence validation of *CNDP2*-KO cell clones

Genomic DNA of cell clones was extracted using 50 μL of Direct PCR lysis reagent (Viagene, USA), supplemented with 2.5 μg/mL Proteinase K (AppliChem, Germany). Cells were transferred into lysis buffer and incubated at 55°C for 15 min followed by 85°C for 15 min. Primer pairs (fwd: GAGATCCCGCTCCCTCCTAT, rev: AGATCTTGCCATTGCCCTCC) were designed for generation of amplicons <450 bp around the target site. Q5 PCR (1× Q5 Reaction Buffer, 200 μM dNTPs, 500 nM forward and reverse primer, 0.02 U/μL Q5 High fidelity Polymerase (NEB, USA) and 1 μL of DNA) was performed using the following settings: 98°C for 30 s, 30 cycles of 98°C—10 s; 69°C—30 s; 72°C—2 min and 72°C for 10 min. PCR products were purified using the innuPREP PCRpure kit (Analytic Jena) and concentration was measured using Qubit 4 Fluorometer (ThermoScientific). 500 ng of purified PCR products were sent for Illumina Amplicon sequencing (Genewiz, USA).

4.4 | Enzyme activity

CN2 activity was assayed for recombinant enzyme, in cell culture and human kidney tissue according to a method described before.[53] In brief, the reaction was initiated by the addition of 1 mM individual dipeptide to the recombinant enzyme (human CNDP2 protein, GeneTex, Irvin, CA), to cell homogenate in optimized RIPA buffer (50 mM Tris/HCl, 0.1% TritonX-100 (v/v), 0.5% Sodium-deoxycholat (w/v), 50 mM NaCl and 20 μM $MnCl_2$, pH 7.5) or human kidney homogenate in specific buffer (20 mM Hepes pH 7.2, 210 mM mannitol, 70 mM sucrose, 50 mM NaCl, 20 μM $MnCl_2$, pH 7.5). The reaction was terminated at pre-determined intervals in liquid nitrogen or by adding 1% trichloroacetic acid depending on the method of amino acid detection.

4.5 | CRISPR/Cas-knock out of *CNDP2* in HK-2 cells relative mRNA expression analysis via qPCR

mRNA was extracted and isolated from cell lysates using RNeasy Mini kit (Quiagen, Venlo, NL). cDNA transcription was performed with the High Capacity cDNA Reverse Transcription Kit (Thermo Fisher Scientific, Waltham, MA). For gene expression analysis, *CNDP2* samples were analyzed with SYBR® Green JumpStar™t *Taq*ReadyMix™ (Sigma-Aldrich, Munich, Germany) via quantitative real time PCR using following primer pairs: fwd AGAAGCCCTGCATCACCTAC, rev CCAAAGAGCCCATCAGCAAAA. For *IMPA1* expression fwd: TGGGAATTCACTGCTGGGAT, rev: TTCGTCGTCTCGTTGCAAAG; *ISYNA1* fwd: CCA AAGTCAAGTCCGTGCTT, rev: CCACGTACGGCACAT ACTTG; *MIOX* fwd: AGAGCTCGGGATGTATCAGC, rev: AACTTGTTGAACTCCCGCAC was used. *B-ACTIN* was used as a housekeeping gene (primer pair: fwd: AGAGCTACGAGCTGCCTGAC, rev: CATCCGCA AAGACCTGTACG). Analysis of the data was performed using the 2^{-ddCT} method.

4.6 | RNA-seq

Total RNA was extracted from HK-2 human kidney tubular cells wild type or subjected to CRISPR-Cas9 mediated *CNDP2*-KO (5 vs. 5 samples) using the total RNA Kit from peqGOLD VWR (VWR, Radnor, PA, USA) with in-column DNase treatment, following the manufacturer's standard protocol. RNA concentration was quantified with a Nanodrop 2000 and the RNA quality was assessed using the Bioanalyzer 2100 with the RNA 6000 nano kit (Agilent). Only samples with RIN (RNA integrity number) >9 were used for RNA-seq library preparation in multiplexing using the Illumina Truseq Stranded mRNA kit. The library has been run on an Illumina Nextseq 500 sequencer. Demultiplexed Fastq files were checked for quality with

the FastQC program and mapped against the GRCh38 human genome with the GENCODE 27 (Ensembl 90) annotation using the STAR (Spliced Transcripts Alignment to a Reference) package. Differentially expressed genes were identified with the DESeq2 package,[54] using the Benjamini-Hochberg (BH) adjustment for false discovery rate (FDR) calculation. Principal Component Analysis (PCA) plot was generated using the plotPCA function of the DESeq2 package. Volcano plot has been obtained using the default scatterplot function of R. Protein coding genes with a FDR < 10% and a log2 (fold change) >2 and <−2 were selected for subsequent analysis. GOterms relative to biological processes (BP) and molecular function (MF) were calculated using the Classic Fisher statistics of the topGO package and were plotted using the ggplot2 package (Bioconductor). Similarly, KEGGS-mapped pathways were calculated on differentially expressed genes using the Fisher statistics. Heatmaps were generated on significant or custom GOterms based on scaled rlog (regularized log transformation) expression values (*z*-score). RNAseq fastq files can be obtained from the Arrayexpress platform (www.ebi.ac.uk/arrayexpress/) under the accession number E-MTAB-11436.

4.7 | Western blotting

Samples were lysed in RIPA buffer and 35–40 µg protein lysate was used for analysis. SDS-PAGE was performed with an 8% or 12% polyacrylamid gel, proteins were transferred to a 0.4 µm nitrocellulose or PDVF (for tight junction protein analysis) membrane. CN2 antibody 14925-1-AP (Proteintech, Manchester, UK) was used in a dilution of 1:2000 overnight at 4°C, tight junction proteins antibodies were diluted 1:1000 (OCCL: 711500, Thermo Fisher Scientific, Waltham, MA; TRIC: 700191 Thermo Fisher Scientific, Waltham, MA; MD3: 25567-1-AP, Proteintech, Manchester, UK; LSR: HPA007270, Atlas antibodies, Bromma Sweden; ILDR1: bs-11013R, Bioss antibodies, Woburn, MA, USA; ILDR2: HPA012545, Sigma Aldrich, Munich, Germany; ZO-1: 61–7300, Thermo Fisher Scientific, Waltham, MA; CLDN1: 519000, Thermo Fisher Scientific, Waltham, MA; CLDN2: 325600, Thermo Fisher Scientific, Waltham, MA; CLDN3: 341700, Thermo Fisher Scientific, Waltham, MA; CLDN7: 349100, Thermo Fisher Scientific, Waltham, MA; CLDN8: 400700Z, Thermo Fisher Scientific, Waltham, MA; CLND10: 38-8400, Thermo Fisher Scientific, Waltham, MA). β-ACTIN (A5441, 1:1000) for tight junction and (A2228 against β-ACTIN; both Sigma Aldrich, Munich, Germany, 1:80 000) for CN2 detection was used (1 h at room temperature). Antibodies for tight junction protein analysis were diluted in 5% BSA in TBST, all other antibodies were diluted in 5% no-fat dry milk in PBST. Densitometric quantification of western blotting results was performed using the ImageJ Fiji application and normalized to the respective reference.

4.8 | MTT cell viability assay

Cell viability was measured with an MTT assay. In brief, confluent cells were detached with trypsin (Thermo Fisher Scientific, Waltham, MA) and seeded on 96-well plates followed by an overnight growth phase. After 48 h, 50 µL PBS (Thermo Fisher Scientific, Waltham, MA) with 2 mg/mL 3-(4,5-dimethylthiazol-2-yl)-2,5-diphenyltetrazolium bromide (MTT) was added and discarded after 4 h, cells were lysed with 200 µL DMSO per well (1 h). The absorption of the solution was measured spectrophotometrically at 590 nm (background was measured at 620 nm and subtracted).

4.9 | Stress conditions

Experiments simulating stress conditions were all performed in 0.1% fetal calf serum media with 1% penicillin and streptomycin (v/v). Oxidative stress was induced by incubation with 0.3, 3 and 6 nM $FeSO_4$ and 0.05, 0.5 and 1 mM H_2O_2 (Fenton reagent) for 24 h. Treatment with 0.1, 0.2, 0.3 or 0.4 µM Ferrostatin-1 was performed over 48 h. Ammonium ferric citrate (FAC) was used to simulate ferroptosis; glucose stress was simulated by increasing glucose concentrations; treatment duration was over 24 h.

4.10 | Cell proliferation assay (BrdU)

Cell proliferation rate was determined with the Assay Cell proliferation Elisa BrdU (Roche, Basel, Swiss) following precisely manufacturing protocol. 5000 to 313 HK-2 WT and *CNDP2*-KO cells per well were seeded into a 96 well plate following 2-fold serial dilution and cells were adhered overnight under 10% FCS media condition. Cells were washed with DPBS following incubation with media containing 0.1% FCS for 24 h. Incubation with BrdU labelling solution was performed for additional 24 h, and measurements were performed photometrically at 370 nm 5 min after adding the substrate solution to the wells. For evaluation, proliferation rate of 1250 cells seeded per well was used.

4.11 | FACS

The size and granularity in HK-2 WT and *CNDP2*-KO cells was analyzed by flow cytometry. Cells were centrifuged for

5 min at 300 *g*, 4°C and in PBS with 1% FCS resuspended for analysis. Measurements were performed using an LSR II cytometer (BD Biosciences, Heidelberg, Germany) and analyzed by FACS Diva (Becton Dickinson, San Jose, CA, USA) and FlowJo software version 10.1r5 (Ashland, OR, USA). Cell size and granularity were determined by forward Scatter (FSC) and side scatter (SSC).

4.12 | Metabolomics

A panel of 18 amino acids were determined as previously described by Weger et al.[55] including alanine (Ala), arginine (Arg), asparagine (Asn), aspartate (Asp), glutamine (Gln), glutamate (Glu), glycine (Gly), histidine (His), isoleucine (Ile), leucine (Leu), lysine (Lys), methionine (Met), phenylalanine (Phe), proline (Pro), serine (Ser), threonine (Thr), tyrosine (Tyr) and valine (Val). Cysteine (Cys) was determined after derivatization with monobromobimane on a Hypersil™ ODS C18-Column (Thermo Fisher Scientific, Waltham, MA).[56] 35 dipeptides were determined by an UPLC-MS/MS method as described by Heidenreich[28] or by HPLC after derivatization.[56] Alanyl-Alanine (Ala-Ala), Alanyl-Glutamine (Ala-Gln), Alanyl-Glutamate (Ala-Glu), Alanyl-Glycine (Ala-Gly), Alanyl-Histidine (Ala-His), Alanyl-Phenylalanine (Ala-Phe), Alanyl-Proline (Ala-Pro), Alanyl-Tyrosine (Ala-Tyr), Anserine, Arginyl-Phenylalanine (Arg-Phe), Aspartyl-Glutamine (Asp-Gln), Carnosine, Glutamyl-Glutamate (Glu-Glu), γ-Glutamyl-ε-Lysine (γ-Glu-ε-Lys), Glycyl-Aspartate (Gly-Asp), Glycyl-Glutamate (Gly-Glu), Glycyl-Histidine (Gly-His), Glycyl-Leucine (Gly-Leu), Glycyl-Phenylalanine (Gly-Phe), Glycyl-Proline (Gly-Pro), Histidyl-Alanine (His-Ala), Histidyl-Leucine (His-Leu), Histidyl-Serine (His-Ser), Leucyl-Histidine (Leu-His), Leucyl-Proline (Leu-Pro), Phenylalanine-Alanine (Phe-Ala), Prolyl-Glycine (Pro-Gly), Prolyl-Leucine (Pro-Leu), Seryl-Alanine (Ser-Ala), Seryl-Glutamine (Ser-Gln), Seryl-Histidine (Ser-His), Tyrosyl-Alanine (Tyr-Ala), Tyrosyl-Phenylalanine (Tyr-Phe), Valyl-Tyrosine (Val-Tyr) were measured vie UPLC-MS/MS method, Cys-Gly by HPLC on a Hypersil™ ODS C18-Column. Glutathione (GSH) was measured after derivatization[56] by HPLC on a Spherisorb ODS1 C18-Column (Waters, Mildford, MA). Analyses of cell pellets via MxP® Quant 500 metabolomics kit (Biocrates) were carried out as described by Andresen et al after MTBE/EtOH extraction.[57]

4.13 | Gas chromatography/mass spectrometry (GC/MS) analysis

From frozen cell pellets (5×10^6 cells), sample material was extracted with 180 µL 100% methanol (HPLC-grade) containing 10 µL 0.02 mg/mL Ribitol (Sigma A5502) and 10 µL 0.2 mg/mL Heptadecanoic acid (C17:0, Sigma H3500) as internal standards for 15 min. at 70°C with vigorous shaking. After addition of 100 µL 100% chloroform (HPLC-grade), samples were shaken for 5 min at 37°C. To separate polar and organic phases, 200 µL HPLC-grade water were added and samples were centrifuged for 10 min at 11 000 *g*. While avoiding the interphase containing insoluble matter, 300 µL of the polar (upper) phase were transferred to a short thread glass vial with 0.2 µL microinsert and dried using a vacuum concentrator (Eppendorf Concentrator Plus) without heating.

Sequential on-line methoximation and silylation reactions were performed using an MPS autosampler (Gerstel, Mülheim Ruhr). Methoximation was performed by adding 20 µL 20 mg/mL methoxyamine hydrochloride (Sigma 226904) in pyridine (Sigma 270970) and incubation at 37°C for 90 min in an MPS Agitator Unit (250 rpm). For silylation reactions, 45 µL of N-Methyl-N-(trimethylsilyl)trifluoroacetamide (MSTFA; Sigma 69479) were added and samples were incubated at 37°C for 30 min with gentle shaking. Before injection, samples were incubated for 45 min at RT.

For GC/MS analysis, a GC-ToF system was used consisting of an Agilent 7890 Gas Chromatograph (Agilent, Santa Clara) fitted with a Rxi-5Sil MS column (30 m × 0.25 mm × 0.25 µm; Restek) coupled to a Pegasus BT Mass Spectrometer (LECO). The GC was operated with an injection temperature of 250°C and 1 µL sample was injected with a split ratio of 10. The GC temperature program started with a 1 min. hold at 40°C followed by a 6°C/min ramp up to 210°C, a 20°C/min ramp up to 330°C and a bake-out at 330°C for 5 min. using Helium as carrier gas with constant linear velocity. The ToF mass spectrometer was operated with ion source and interface temperatures of 250°C, a solvent cut time of 9 min and a scan range (m/z) of 50–600 with an acquisition rate of 17 spectra/s. The ChromaTof v5.50 software (LECO Corporation, Michigan) was used for data processing.

To analyze total fatty acids, 80 µL of the lower organic phase after extraction were transferred to a glass vial and dried in a speed-vac without heating. For transmethylation reactions, pellets were re-dissolved in 40 µL TBME (tert-Butyl methyl ether, Sigma) and 20 µL TMSH (Trimethylsulfoniumhydroxid, Sigma), incubated for 45 min. at 50°C and analyzed using a GC/MS-QP2010 Plus (Shimadzu®) fitted with a Zebron ZB 5MS column (Phenomenex®; 30 m × 0.25 mm × 0.25 µm) for fatty acid methyl esters (FAME). The GC was operated with an injection temperature of 230°C, 1 µL sample was injected with split mode (1:10). The GC temperature started with 40°C (1 min) followed by a 6°C/min ramp to 210°C, a 20°C/min ramp to 330°C and a bake-out for 5 min. at 330°C using Helium as carrier gas with constant linear velocity. The MS

was operated with ion source and interface temperatures of 250°C, a solvent cut time of 7 min and a scan range (m/z) of 40–700 with an event time of 0.2 s. The "GCMS solution" software (Shimadzu®) was used for data processing.

4.14 | Transepithelial electric resistance (TER)

Tubular cell monolayer integrity and barrier function was assessed as described previously.[58] In brief, a cell suspension (5×10^4 cells/cm^2) was seeded and cultured on a polyester mesh transwell filter (0.4 μm pore size, 12-well type; Costar. MA. USA) under normal culture conditions. The inner and outer chambers of the Transwell were filled with 0.2 mL and 1 mL culture medium, respectively. TER was measured daily using an EVOM volt/ohm meter with STX-2 electrodes (World Precision Instruments, Sarasota, FL, USA). To calculate the normalized TER of each monolayer. Background TER of a blank filter was subtracted from the TER of the respective cell monolayer. To compare baseline TER of WT HK-2 and *CNDP2*-KO HK-2 cells, TER was measured daily for up to 21 days, and the medium was changed every 3–4 days. The treatment of WT HK-2 with dipeptides was initiated. when the monolayer was formed and differentiated as demonstrated by a plateau in the TER (around 5 days post-seeding).

4.15 | Paracellular permeability analysis of HK-2 monolayers

The paracellular permeability of HK-2 monolayers was determined by measuring concentrations changes of fluorescein isothiocyanate (FITC) labeled 10 kDa dextran and 66 kDa albumin (Sigma-Aldrich, St. Louis, MO, USA) in the lower transwell compartment, following their addition to the upper compartment at a concentration 1 mg/mL. An equimolar amount of unlabeled dextran was added to the lower compartment of the Transwell to maintain isotonic conditions. Calibration curves were established from FITC dextran stock solutions and sample fluorescence was determined using a fluorescence spectrophotometer (F-2000; Hitachi, Tokyo, Japan) at an excitation wavelength of 490 nm and an emission wavelength of 520 nm in one black 96 well plate (Greiner, Nürtingen, Germany). Solute permeability coefficients (SPC; m/s) were calculated using the following formula:

$$\mathrm{SPC} = -\frac{4V}{\Delta t A}\ln\frac{\mathrm{Cu0}-4\mathrm{Cl4}}{\mathrm{Cu0}-4\mathrm{Cl2}}$$

where V is the volume of the lower compartment (m^3), A the membrane area (m^2), Δt the time interval (s), and C the concentration of the molecular marker (Cu0 = concentration at the upper side at time 0; Cl4 = concentration at the lower side at 4 h; Cl2 = concentration at the lower side at 2 h).

4.16 | Determination of NHE activity

To measure the transport activity of NHEs, the pH-dependent fluorescence of acridine orange was used. Cells were seeded in same amounts on 96-well plates and grown to confluence. Medium was replaced by sodium-free preincubation buffer (280 mM Mannitol, 5 mM MES, 2 mM $MgCl_2$, pH 5.5) with or without 10 μM EIPA (5-(N-Ethyl-N-isopropyl)amiloride), which inhibits several NHEs completely or in parts,[59] for 2 h. The buffer was then replaced by sodium-free measuring buffer (240 mM Mannitol, 20 mM HEPES, 2 mM $MgCl_2$, 6 μM acridine orange, pH 7.5) with or without the 10 μM EIPA. Emission shifts at 530 nm were detected for 1 min after addition of Na-Gluconate (final concentration 100 mM) in a plate reader (Tecan Infinite M200, Tecan, Switzerland, 493 nm excitation and 530 nm emission), and slopes of intensity changes were compared between wildtype and CN2-KO cells in the absence or presence of the NHE3 inhibitor EIPA.

4.17 | Dilution potentials

Cells grown on transwell filters were mounted into Ussing chambers with an area of 0.6 cm^2. Resistance of bathing solutions was measured prior to each experiment and subtracted. Ussing chambers and water-jacketed gas lifts were filled with 10 mL standard Ringer's solution (in mM: Na^+ 140; Cl^- 149.8; K^+ 5.4; Ca^{2+} 1.2; Mg^{2+} 1; HEPES 10; D(+)-glucose 10, D(+)-mannose 10, beta-hydroxybutyric acid 0.5, and L-glutamine 2.5 mmol/L, pH 7.4). The solution was equilibrated with 5% CO_2 and 95% O_2 at 37°C. Potential changes were recorded by switching the solution of one hemi chamber to a solution containing a reduced concentration of NaCl and all other components identical to standard Ringer's. Osmolality was balanced by mannitol. The resulting dilution potentials were used for calculations using the Goldman-Hodgkin-Katz equation as reported before.[43,60,61]

4.18 | Ion secretion/transport via cystic fibrosis transmembrane conductance regulator (CFTR) and glucose transport via sodium-glucose linked transporters 1 and 2 (SGLT1/2)

Cells grown on transwell filters were mounted into Ussing chambers in glucose-free Ringer's solution. Changes in short-circuit current (I_{SC}) were recorded and used for

calculation of transporter activity depending on ions. CFTR activity was determined by stimulating Cl^- secretion by 10 μmol/L forskolin, inhibiting CFTR then with 10 μmol/L 5-nitro-2-(3-phenylpropylamino) benzoic acid (NPPB) and stimulating again to derive noninhibitable fractions. For glucose transport, transport via SGLT1/2 was stimulated by addition of glucose (100 mM 1 mL/5 mL apical bathing solution). After 20 min, phlorizin was added apically, and after further 20 min, again glucose was added to derive non-inhibitable fractions.

4.19 | Immunostaining

HK-2 cells were cultured on chamber slides (Nunc, Langenselbold, Germany) and Transwell (Costar, MA, USA). Cells were fixed with absolute ethanol (5 min, −20°C), blocked with 5% BSA in PBS (1 h, 37°C), incubated with primary antibodies overnight at 4°C (ZO1 MA3-39100-A555, Thermo Fisher Scientific, Waltham, MA, USA; dilution 1:1000, SGLT2 ab8526, NHE ab90630, both from Abcam, Cambridge, UK both in 1:500 dilution and AQP1 sc-32738 from Santa Cruz, Heidelberg, Germany dilution 1:500). After washing, secondary AlexaFluor 555 or 647 antibody was added (overnight, 4°C). Nuclei were visualized by 4′,6-Diamidin-2-phenylindol (DAPI) staining (15 min at room temperature) and chamber slides were fixed with ProlongGold (Thermo Fischer Scientific, Waltham, USA). Stainings were analyzed by fluorescence microscopy (ACQUIFER Imaging GmbH, Heidelberg, Germany) or confocal microscopy (Carl Zeiss LSM700, scanning laser confocal microscope, Jena, Germany; Leica TCS SP5, Leica Biosystems, Wetzlar, Germany) with equal exposure times, gray scale images were quantified as described previously.[58,62] Immunohistochemical stainings against CN2 in paraffin embedded human kidney tissue sections were performed using an anti-CNDP2 antibody (Proteintech, Rosemont, USA, 14925-1-AP, dilution 1:1000). For densitometrical analysis of human tissue sections glomeruli were excluded, evaluations were performed using Aperio image scope software (Leica, Wetzlar, Germany).

4.20 | Mice and human tissues

Wildtype mice (C57BL/6J) were housed in the Interfaculty Biomedical Facility (IBF) at Heidelberg University. Food and water were supplied ad libitum. At sacrifice (age 40 weeks), kidney, lung, liver and pancreas were harvested, formalin fixed and paraffin embedded for histopathology. The studies were approved by the respective authorities (Regierungspräsidium Karlsruhe, Germany, 35–9165 81/G-209/16).

Human tissue samples were provided by the Tissue Bank of the National Center for Tumor Diseases (NCT), Heidelberg, Germany, in accordance with the regulations of the tissue bank and the approval of the ethics committee of Heidelberg University (S-284/2018). Immunohistochemical staining against CN2 was performed in tissue microarrays (TMAs).

Cryo-conserved samples were used for dipeptides and amino acid analysis, mRNA und protein expression analysis via qPCR and western blotting enzymatic activity. Analysis were performed as described in the respective paragraphs.

4.21 | Statistics

All experiments were performed at least in three biological replicates, including 3 to 16 technical replicates. All data are presented as mean ± SD, if not stated otherwise. Student's *t*-test or if three or more groups were tested against each other one-way ANOVA were performed. Outliers for experiments with human kidney tissue were identified using robust regression and outlier removal (ROUT) method with $Q = 1$. Statistical analysis was performed using GraphPad Prism 9 software. Evaluation of RNA-seq data see corresponding paragraph. Two sided tests were used, and p value <0.05 was considered significant.

5 | CONCLUSION

In conclusion, CN2-mediated DP degradation has major impact on the metabolic profile of human proximal tubular cells. CN2 deficiency substantially compromises DP, AA and associated metabolic pathways, reduces energy status, cell viability and proliferation, and alters essential tubular cell transport functions, altogether indicating a key role of CN2 enzyme, that already can be connected to known kidney pathologies. Our findings implicate the necessity for in vivo modulation of CN2, which will elucidate the functional role of CN2 under physiological and pathophysiological conditions. Understanding of CN2 regulation bears promising therapeutic potential.

AUTHOR CONTRIBUTIONS

Tilman Pfeffer: Conceptualization; investigation; formal analysis; visualization; validation; methodology. **Susanne M. Krug:** Conceptualization; methodology; writing – review and editing; visualization; investigation; writing – original draft. **Tamara Kracke:** Methodology; data curation; investigation. **Robin Schürfeld:** Data curation; methodology; investigation. **Florian Colbatzky:**

Methodology; data curation; investigation. **Philip Kirschner:** Methodology; data curation; investigation. **Rebekka Medert:** Methodology. **Marc Freichel:** Methodology; project administration. **Dagmar Schumacher:** Methodology. **Maria Bartosova:** Methodology; writing – review and editing; visualization; validation; data curation; resources; investigation. **Sotiris G. Zarogiannis:** Methodology. **Martina U. Muckenthaler:** Methodology. **Sandro Altamura:** Methodology; data curation. **Silvia Pezer:** Methodology; data curation. **Nadine Volk:** Methodology; visualization. **Constantin Schwab:** Methodology; visualization; investigation. **Stefan Duensing:** Methodology; visualization; investigation. **Thomas Fleming:** Methodology; visualization; data curation; investigation. **Elena Heidenreich:** Methodology; data curation; software; investigation. **Johannes Zschocke:** Writing – original draft; conceptualization. **Rüdiger Hell:** Conceptualization; visualization; methodology. **Gernot Poschet:** Methodology; visualization; validation; investigation. **Claus P. Schmitt:** Conceptualization; investigation; writing – original draft; funding acquisition; writing – review and editing; project administration; supervision. **Verena Peters:** Supervision; project administration; writing – review and editing; visualization; methodology; conceptualization; funding acquisition; writing – original draft.

ACKNOWLEDGMENTS

We thank Kristina Klingbeil for technical assistance. Open Access funding enabled and organized by Projekt DEAL.

FUNDING INFORMATION

This study was supported by grants from the Deutsche Forschungsgemeinschaft (DFG, German Research Foundation)—Project number 236360313—CRC 1118. M. Bartosova was funded by the Olympia Morata Program of Heidelberg University and acknowledges Baden-Württemberg Stiftung for the financial support by the Eliteprogramme for Postdocs.

CONFLICT OF INTEREST STATEMENT

The authors have no conflicts of interest relevant to the content of this article.

DATA AVAILABILITY STATEMENT

RNAseq fastq files can be obtained from the Arrayexpress platform www.ebi.ac.uk/arrayexpress/ under the accession number E-MTAB-11436.

ANIMAL STUDIES

The animal studies were approved by the respective authorities (Regierungspräsidium Karlsruhe, Germany, 35-9165.81/G-209/16) and performed according to guidelines (ARRIVE).

ORCID

Tilman Pfeffer https://orcid.org/0000-0003-1502-426X
Susanne M. Krug https://orcid.org/0000-0002-1293-2484
Philip Kirschner https://orcid.org/0000-0002-6711-5959
Verena Peters https://orcid.org/0000-0002-4649-0848

REFERENCES

1. Bartosova M, Herzog R, Ridinger D, et al. Alanyl-glutamine restores tight junction organization after disruption by a conventional peritoneal dialysis fluid. *Biomolecules*. 2020;10(8):1178.
2. Moreno JC, Rojas BE, Vicente R, et al. Tyr-asp inhibition of glyceraldehyde 3-phosphate dehydrogenase affects plant redox metabolism. *EMBO J*. 2021;40:e106800.
3. Boldyrev AA, Aldini G, Derave W. Physiology and pathophysiology of carnosine. *Physiol Rev*. 2013;93(4):1803-1845.
4. Weigand T, Colbatzky F, Pfeffer T, et al. A global Cndp1-Knockout selectively increases renal carnosine and anserine concentrations in an age- and gender-specific manner in mice. *Int J Mol Sci*. 2020;21(14):4887.
5. Kaur H, Kumar C, Junot C, Toledano MB, Bachhawat AK. Dug1p is a Cys-Gly peptidase of the gamma-glutamyl cycle of *Saccharomyces cerevisiae* and represents a novel family of Cys-Gly peptidases. *J Biol Chem*. 2009;284(21):14493-14502.
6. Kobayashi S, Homma T, Okumura N, et al. Carnosine dipeptidase II (CNDP2) protects cells under cysteine insufficiency by hydrolyzing glutathione-related peptides. *Free Radic Biol Med*. 2021;174:12-27.
7. Kim JT, Li VL, Terrell SM, Fischer CR, Long JZ. Family-wide annotation of enzymatic pathways by parallel in vivo metabolomics. *Cell Chem Biol*. 2019;26(11):1623-1629.e3.
8. Jansen RS, Addie R, Merkx R, et al. N-lactoyl-amino acids are ubiquitous metabolites that originate from CNDP2-mediated reverse proteolysis of lactate and amino acids. *Proc Natl Acad Sci USA*. 2015;112(21):6601-6606.
9. Li VL, He Y, Contrepois K, et al. An exercise-inducible metabolite that suppresses feeding and obesity. *Nature*. 2022;606(7915):785-790.
10. Ahluwalia TS, Lindholm E, Groop LC. Common variants in CNDP1 and CNDP2, and risk of nephropathy in type 2 diabetes. *Diabetologia*. 2011;54(9):2295-2302.
11. McDonough C, Hicks PJ, Lu L, Langefeld CD, Freedman BI, Bowden DW. The influence of carnosinase gene polymorphisms on diabetic nephropathy risk in African-Americans. *Hum Genet*. 2009;126:265-275.
12. Di Meo A, Batruch I, Brown MD, et al. Searching for prognostic biomarkers for small renal masses in the urinary proteome. *Int J Cancer*. 2020;146(8):2315-2325.
13. Vu HM, Mohammad HB, Nguyen TNC, et al. Quantitative proteomic analysis of bronchoalveolar lavage fluids from patients with small cell lung cancers. *Proteomics Clin Appl*. 2023;17:e2300011.
14. Zhang LQ, Yang HQ, Yang SQ, et al. CNDP2 acts as an activator for human ovarian cancer growth and metastasis via the PI3K/AKT pathway. *Technol Cancer Res Treat*. 2019;18:1533033819874773.

15. Speed JS, Fox BM, Johnston JG, Pollock DM. Endothelin and renal ion and water transport. *Semin Nephrol*. 2015;35(2):137-144.
16. van de Poll MC, Soeters PB, Deutz NE, Fearon KC, Dejong CH. Renal metabolism of amino acids: its role in interorgan amino acid exchange. *Am J Clin Nutr*. 2004;79(2):185-197.
17. Nakamura M, Satoh N, Horita S, Nangaku M. Insulin-induced mTOR signaling and gluconeogenesis in renal proximal tubules: a mini-review of current evidence and therapeutic potential. *Front Pharmacol*. 2022;13:1015204.
18. Li H, Dai W, Liu Z, He L. Renal proximal tubular cells: a new site for targeted delivery therapy of diabetic kidney disease. 2022;15(12):1494.
19. Mohandes S, Doke T, Hu H, Mukhi D, Dhillon P, Susztak K. Molecular pathways that drive diabetic kidney disease. *J Clin Invest*. 2023;133(4):e165654.
20. Garibotto G, Tessari P, Sacco P, Deferrari G. Amino acid metabolism, substrate availability and the control of protein dynamics in the human kidney. *J Nephrol*. 1999;12(4):203-211.
21. Nowak KL, Hopp K. Metabolic reprogramming in autosomal dominant polycystic kidney disease: evidence and therapeutic potential. *Clin J Am Soc Nephrol*. 2020;15(4):577-584.
22. Asghari G, Teymoori F, Farhadnejad H, Mirmiran P, Azizi F. Dietary amino acid patterns are associated with incidence of chronic kidney disease. *J Ren Nutr*. 2022;32(3):312-318.
23. Butler M, van der Meer LT, van Leeuwen FN. Amino acid depletion therapies: starving cancer cells to death. *Trends Endocrinol Metab*. 2021;32(6):367-381.
24. Pfeffer T, Wetzel C, Kirschner P, et al. Carnosinase-1 Knock-out reduces kidney fibrosis in Type-1 diabetic mice on high fat diet. *Antioxidants (Basel, Switzerland)*. 2023;12(6):1270.
25. Peters V, Schmitt CP, Weigand T, et al. Allosteric inhibition of carnosinase (CN1) by inducing a conformational shift. *J Enzyme Inhib Med Chem*. 2017;32(1):1102-1110.
26. Peters V, Klessens CQ, Baelde HJ, et al. Intrinsic carnosine metabolism in the human kidney. *Amino Acids*. 2015;47:2541-2550.
27. Lazareth H, Lenoir O, Tharaux PL. Parietal epithelial cells role in repair versus scarring after glomerular injury. *Curr Opin Nephrol Hypertens*. 2020;29(3):293-301.
28. Heidenreich E, Pfeffer T, Kracke T, et al. A novel UPLC-MS/MS method identifies organ-specific dipeptide profiles. *Int J Mol Sci*. 2021;22(18):9979.
29. Kandasamy P, Gyimesi G, Kanai Y, Hediger MA. Amino acid transporters revisited: new views in health and disease. *Trends Biochem Sci*. 2018;43(10):752-789.
30. Valdivielso JM, Eritja À, Caus M, Bozic M. Glutamate-gated NMDA receptors: insights into the function and signaling in the kidney. *Biomolecules*. 2020;10(7):1051.
31. Jappar D, Hu Y, Keep RF, Smith DE. Transport mechanisms of carnosine in SKPT cells: contribution of apical and basolateral membrane transporters. *Pharm Res*. 2009;26(1):172-181.
32. Alghamdi OA, King N, Jones GL, Moens PDJ. Kinetic measurements of Di- and tripeptide and peptidomimetic drug transport in different kidney regions using the fluorescent membrane potential-sensitive dye, DiS-C(3)-(3). *J Membr Biol*. 2017;250(6):641-649.
33. Smith DE, Clémençon B, Hediger MA. Proton-coupled oligopeptide transporter family SLC15: physiological, pharmacological and pathological implications. *Mol Asp Med*. 2013;34(2–3):323-336.
34. Makrides V, Camargo SM, Verrey F. Transport of amino acids in the kidney. *Compr Physiol*. 2014;4(1):367-403.
35. Zietek T, Giesbertz P, Ewers M, et al. Organoids to study intestinal nutrient transport, drug uptake and metabolism - update to the human model and expansion of applications. *Front Bioeng Biotechnol*. 2020;8:577656.
36. Long KR, Rbaibi Y, Bondi CD, et al. Cubilin-, megalin-, and Dab2-dependent transcription revealed by CRISPR/Cas9 knockout in kidney proximal tubule cells. *Am J Physiol Renal Physiol*. 2022;322(1):F14-F26.
37. Li X, Zheng S, Wu G. Amino acid metabolism in the kidneys: nutritional and physiological significance. *Adv Exp Med Biol*. 2020;1265:71-95.
38. Marini HR, Facchini BA, di Francia R, et al. Glutathione: lights and shadows in cancer patients. *Biomedicine*. 2023;11(8):2226.
39. Chen TK, Knicely DH, Grams ME. Chronic kidney disease diagnosis and management: a review. *JAMA*. 2019;322(13):1294-1304.
40. Fromm M, Piontek J, Rosenthal R, Günzel D, Krug SM. Tight junctions of the proximal tubule and their channel proteins. *Pflugers Arch*. 2017;469(7–8):877-887.
41. Furuse M, Hata M, Furuse K, et al. Claudin-based tight junctions are crucial for the mammalian epidermal barrier: a lesson from claudin-1-deficient mice. *J Cell Biol*. 2002;156(6):1099-1111.
42. Milatz S, Krug SM, Rosenthal R, et al. Claudin-3 acts as a sealing component of the tight junction for ions of either charge and uncharged solutes. *Biochim Biophys Acta*. 2010;1798(11):2048-2057.
43. Amasheh S, Meiri N, Gitter AH, et al. Claudin-2 expression induces cation-selective channels in tight junctions of epithelial cells. *J Cell Sci*. 2002;115(Pt 24):4969-4976.
44. Yu AS, Enck AH, Lencer WI, Schneeberger EE. Claudin-8 expression in Madin-Darby canine kidney cells augments the paracellular barrier to cation permeation. *J Biol Chem*. 2003;278(19):17350-17359.
45. Angelow S, Kim KJ, Yu AS. Claudin-8 modulates paracellular permeability to acidic and basic ions in MDCK II cells. *J Physiol*. 2006;571(Pt 1):15-26.
46. Chmiel TA, Gardel ML. Confluence and tight junction dependence of volume regulation in epithelial tissue. *Mol Biol Cell*. 2022;33(11):ar98.
47. Haas AJ, Zihni C, Krug SM, et al. ZO-1 guides tight junction assembly and epithelial morphogenesis via cytoskeletal tension-dependent and -independent functions. *Cells*. 2022;11(23):3775.
48. Nayak B, Xie P, Akagi S, et al. Modulation of renal-specific oxidoreductase/myo-inositol oxygenase by high-glucose ambience. *Proc Natl Acad Sci USA*. 2005;102(50):17952-17957.
49. Prabhu KS, Arner RJ, Vunta H, Reddy CC. Up-regulation of human myo-inositol oxygenase by hyperosmotic stress in renal proximal tubular epithelial cells. *J Biol Chem*. 2005;280(20):19895-19901.
50. Spires D, Manis AD, Staruschenko A. Ion channels and transporters in diabetic kidney disease. *Curr Top Membr*. 2019;83:353-396.
51. Edwards JC. Chloride transport. *Compr Physiol*. 2012;2(2):1061-1092.
52. Ran FA, Hsu PD, Wright J, Agarwala V, Scott DA, Zhang F. Genome engineering using the CRISPR-Cas9 system. *Nat Protoc*. 2013;8(11):2281-2308.
53. Teufel M, Saudek V, Ledig JP, et al. Sequence identification and characterization of human carnosinase and a closely related non-specific dipeptidase. *J Biol Chem*. 2003;278(8):6251-6531.

54. Love MI, Huber W, Anders S. Moderated estimation of fold change and dispersion for RNA-seq data with DESeq2. *Genome Biol*. 2014;15(12):550.
55. Weger BD, Weger M, Gorling B, et al. Extensive regulation of diurnal transcription and metabolism by glucocorticoids. *PLoS Genet*. 2016;12(12):e1006512.
56. Fiskerstrand T, Refsum H, Kvalheim G, Ueland PM. Homocysteine and other thiols in plasma and urine: automated determination and sample stability. *Clin Chem*. 1993;39(2):263-271.
57. Andresen C, Boch T, Gegner HM, et al. Comparison of extraction methods for intracellular metabolomics of human tissues. *Front Mol Biosci*. 2022;9:932261.
58. Bartosova M, Ridinger D, Marinovic I, et al. An experimental workflow for studying barrier integrity, permeability, and tight junction composition and localization in a single endothelial cell monolayer: proof of concept. *Int J Mol Sci*. 2021;22(15):8178.
59. Masereel B, Pochet L, Laeckmann D. An overview of inhibitors of Na(+)/H(+) exchanger. *Eur J Med Chem*. 2003;38(6):547-554.
60. Günzel D, Amasheh S, Pfaffenbach S, et al. Claudin-16 affects transcellular Cl- secretion in MDCK cells. *J Physiol*. 2009;587(Pt 15):3777-3793.
61. Yu AS, Cheng MH, Angelow S, et al. Molecular basis for cation selectivity in claudin-2-based paracellular pores: identification of an electrostatic interaction site. *J Gen Physiol*. 2009;133(1):111-127.
62. Schindelin J, Arganda-Carreras I, Frise E, et al. Fiji: an open-source platform for biological-image analysis. *Nat Methods*. 2012;9(7):676-682.

SUPPORTING INFORMATION

Additional supporting information can be found online in the Supporting Information section at the end of this article.

How to cite this article: Pfeffer T, Krug SM, Kracke T, et al. Knock-out of dipeptidase CN2 in human proximal tubular cells disrupts dipeptide and amino acid homeostasis and para- and transcellular solute transport. *Acta Physiol*. 2024;240:e14126. doi:10.1111/apha.14126